Photon emission in neutral-current interactions at intermediate energies

E. Wang
Departamento de Física Teórica and IFIC, Centro Mixto Universidad de Valencia-CSIC, Institutos de Investigación de Paterna, E-46071 Valencia, Spain

L. Alvarez-Ruso and J. Nieves
Instituto de Física Corpuscular (IFIC), Centro Mixto CSIC-Universidad de Valencia, Institutos de Investigación de Paterna, E-46071 Valencia, Spain

(Received 14 November 2013; published 30 January 2014)

Neutral-current photon emission reactions with nucleons and nuclei are studied. These processes are important backgrounds for $\nu_\mu \to \nu_e$ ($\bar{\nu}_\mu \to \bar{\nu}_e$) appearance oscillation experiments where electromagnetic showers instigated by electrons (positrons) and photons are not distinguishable. At intermediate energies, these reactions are dominated by the weak excitation of the $\Delta(1232)$ resonance and its subsequent decay into $N\gamma$. There are also nonresonant contributions that, close to threshold, are fully determined by the effective chiral Lagrangian of strong interactions. In addition, we have also included mechanisms mediated by nucleon excitations (N^*) from the second resonance region above the $\Delta(1232)$. From these states, the contribution of the D_{13} $N^*(1520)$ turns out to be sizable for (anti)neutrino energies above 1.5 GeV. We have extended the model to nuclear targets taking into account Pauli blocking, Fermi motion, and the in-medium Δ resonance broadening. We present our predictions for both the incoherent and coherent channels, showing the relevance of the nuclear corrections. We also discuss the target mass dependence of the cross sections. This study is important to reduce systematic effects in neutrino oscillation experiments.

DOI: 10.1103/PhysRevC.89.015503 PACS number(s): 25.30.Pt, 23.40.Bw, 13.15.+g, 12.39.Fe

I. INTRODUCTION

A good understanding of (anti)neutrino cross sections is crucial to reduce the systematic uncertainties in oscillation experiments aiming at a precise determination of neutrino properties [1]. Our present knowledge of neutrino-nucleus interactions has been significantly improved by a new generation of oscillation and cross-section experiments. Quasielastic (QE) scattering measurements have been published by MiniBooNE [2–4] at neutrino energies $E_\nu \sim 1$ GeV, by MINERνA [5,6] at $E_\nu \sim 3.5$ GeV, and by NOMAD at high (3–100 GeV) energies [7]. Detailed single pion production data have become available from MiniBooNE [8–10] for different reaction channels including the coherent one, which was also studied by SciBooNE [11,12] at $E_\nu \sim 1$ GeV and NOMAD [13]. Finally, new inclusive cross-section results have been reported by T2K [14], SciBooNE [15], MINOS [16], and NOMAD [17] Collaborations. These results challenge our understanding of neutrino interactions with matter and have triggered a renewed theoretical interest [18]. Quasielastic scattering has been investigated with a local Fermi gas [19–22], realistic spectral functions [23,24], different models to describe the interaction of the knocked-out nucleon with the residual nucleus [25–27], and using the information from electron scattering data encoded in the scaling function [28]. The importance of two-nucleon contributions for the proper understanding of QE-like and inclusive cross sections has emerged in different studies [22,29,30], and their impact in the kinematic neutrino-energy reconstruction has been stressed [31–33]. Incoherent pion production has also been scrutinized using microscopic models for the reaction mechanism on the nucleon [34–39], with special attention paid to pion final state interactions in nuclei [39–43]. New microscopic models have been developed for coherent pion production [44–48] while traditional ones, based on the partial conservation of the axial current (PCAC), have been updated [49–52].

One of the possible reaction channels is photon emission induced by neutral-current (NC) interactions (NCγ), which can occur on single nucleons and on nuclear targets. Weak photon emission has a small cross section compared, for example, with pion production, the most important inelastic mechanism. In spite of this, NC photon emission turns out to be one of the largest backgrounds in $\nu_\mu \to \nu_e(\bar{\nu}_\mu \to \bar{\nu}_e)$ oscillation experiments where electromagnetic showers instigated by electrons (positrons) and photons are not distinguishable. Thus, NC events producing single photons become an irreducible background to the charge-current (CC) QE signatures of ν_e ($\bar{\nu}_e$) appearance. This is precisely the case of the MiniBooNE experiment that was designed to test an earlier indication of a $\bar{\nu}_\mu \to \bar{\nu}_e$ oscillation signal observed at LSND [53,54]. The MiniBooNE experiment finds an excess of events with respect to the predicted background in both ν and $\bar{\nu}$ modes. In the $\bar{\nu}$ mode, the data are found to be consistent with $\bar{\nu}_\mu \to \bar{\nu}_e$ oscillations and have some overlap with the LSND result [55]. MiniBooNE data for ν_e appearance in the ν_μ mode show a clear (3σ) excess of signal-like events at low reconstructed neutrino energies ($200 < E_\nu^{\rm QE} < 475$ MeV) [55,56]. However, the $E_\nu^{\rm QE}$ distribution of the events is only marginally compatible with a simple two-neutrino oscillation model [55]. While several exotic explanations for this excess have been proposed, it could be related to unknown systematics or poorly understood backgrounds in the experimental analysis. In a similar way, NCγ is a source of misidentified electronlike

events in the ν_e appearance measurements at T2K [57]. Even if the NCγ contribution to the background is relatively small, it can be critical in measurements of the CP-violating phase. It is therefore very important to have a robust theoretical understanding of the NC photon emission reaction, which cannot be unambiguously constrained by data. This is the goal of the present work.

The first step towards a realistic description of NC photon emission on nuclear targets of neutrino detectors is the study of the corresponding process on the nucleon. Theoretical models for the $\nu N \to \nu N\gamma$ reaction have been presented in Refs. [38,58]. They start from Lorentz-covariant effective field theories with nucleon, pion, $\Delta(1232)$ but also scalar (σ), and vector (ρ, ω) mesons as the relevant degrees of freedom, and exhibit a nonlinear realization of (approximate) $SU(2)_L \otimes SU(2)_R$ chiral symmetry. The single mechanism of $\Delta(1232)$ excitation followed by its decay $\Delta \to N\gamma$ was considered in Ref. [59], where a consistent treatment of the Δ vertices and propagator is adopted. Several features of the previous studies, in particular the approximate chiral symmetry and the dominance of the $\Delta(1232)$ mediated mechanism are common to the model derived in our work. In Ref. [38], a special attention is paid to the power counting, which is shown to be valid for neutrino energies below 550 MeV. However, the neutrino fluxes of most neutrino experiments span to considerably higher energies. Thus, in Ref. [60], the power counting scheme was abandoned, and the model of [38] was phenomenologically extended to the intermediate energies ($E_\nu \sim 1$ GeV) relevant for the MiniBooNE ν flux, by including phenomenological form factors. Although the extension proposed for the Δ and the nucleon Compton-like mechanisms seems reasonable, the one for the contact terms notably increases the cross section above $\sim$1 GeV (they are more significant for neutrinos than for antineutrinos). Because the contact terms and the associated form factors are not well understood so far, the model predictions for $E_\nu > 1$ GeV should be taken cautiously, as explicitly acknowledged in Ref. [60].

In nuclear targets, the reaction can be incoherent when the final nucleus is excited (and fragmented) or coherent, when it remains in the ground state. It is also possible that, after nucleon knockout, the residual excited nucleus decays emitting low-energy γ rays. This mechanism has been recently investigated [61] and shall not be discussed here. The model of Ref. [58] was applied to incoherent photon production in an impulse approximation that ignores nuclear corrections [62]. These are also neglected in the coherent case, which is calculated by treating the nucleus as a scalar particle and introducing a form factor to ensure that the coherence is restricted to low-momentum transfers [58]. More robust is the approach of Refs. [48,63] based on a chiral effective field theory for nuclei, again extended phenomenologically to higher energies [60]. In addition to Pauli blocking and Fermi motion, the Δ resonance broadening in the nucleus, is also taken into account. The latter correction causes a very strong reduction of the resonant contribution to the cross section, in variance with our results, as will be shown below. The ratio of the Δ to photon and Δ to π^0 decay rates is enhanced in the nuclear medium by an amount that depends on the resonance invariant mass, momentum, and also production position inside the nucleus, as estimated with a transport model [64,65]. The coherent channel was also studied in Refs. [66,67] at high energies. A discussion about these works can be found in Sec. VE of Ref. [58].

It is worth mentioning that both the models of Ref. [58] and Refs. [38,48,60,63] have been used to calculate the NCγ events at MiniBooNE with contradicting conclusions [60,62]. Although in Ref. [62] the number of these events were calculated to be twice as many as expected from the MiniBooNE *in situ* estimate, much closer values were predicted in Ref. [60]. The result that NCγ events give a significant contribution to the MiniBooNE low-energy excess [58] could have its origin in the lack of nuclear effects and rather strong detection efficiency correction.

Here we present a realistic model for NC photon emission in the $E_\nu \sim 1$ GeV region that extends and improves certain relevant aspects of the existing descriptions. The model is developed in the line of previous work on weak pion production on nucleons [35] and nuclei for both incoherent [39] and coherent [46,68] processes. The model for free nucleons satisfies the approximate chiral symmetry incorporated in the nonresonant terms and includes the dominant $\Delta(1232)$ excitation mechanism, with couplings and form factors taken from the available phenomenology. Moreover, we have extended the validity of the approach to higher energies by including intermediate excited states from the second resonance region [$P_{11}(1440)$, $D_{13}(1520)$, and $S_{11}(1535)$]. Among them, we have found a considerable contribution of the $D_{13}(1520)$ for (anti)neutrino energies above 1.5 GeV. When the reaction takes place inside the nucleus, we have applied a series of standard medium corrections that have been extensively confronted with experiment in similar processes such as pion [69,70], photon [71], and electron [72,73] scattering with nuclei, or coherent pion photo [74] and electroproduction [75].

This paper is organized as follows. The model for NC production of photons off nucleons is described in Sec. II. After discussing the relevant kinematics, we evaluate the different amplitudes in Sec. II B. In the first place, the dominant $\Delta(1232)$ and nonresonant contributions are studied (Sec. II B 1). Next, we examine the contributions driven by N^* resonances from the second resonance region (Sec. II B 2). The relations between vector form factors and helicity amplitudes, and the off-diagonal N^*N Goldberger-Treiman (GT) relations are discussed in Appendixes A and B, respectively. NCγ reactions in nuclei are studied in Sec. III. First, in Sec. III A, we pay attention to the incoherent channel driven by one particle–one hole (1p1h) nuclear excitations. Next, in Sec. III B, the coherent channel is studied. We present our results in Sec. IV, where we also compare some of our predictions with the corresponding ones from Refs. [58,60]. This section is split in two subsections, where the results for NCγ on single nucleons (Sec. IV A) and on nuclei (Sec. IV B) are discussed. Predictions for nuclear incoherent and coherent reactions are presented in Secs. IV B 1 and IV B 2, respectively. Finally the main conclusions of this work are summarized in Sec. V.

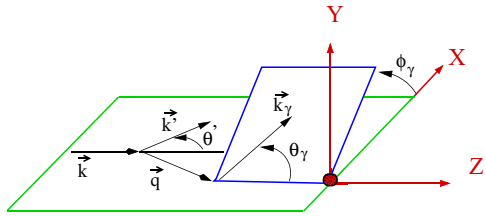

FIG. 1. (Color online) Representation of the different LAB kinematical variables used through this work.

II. NEUTRAL-CURRENT PHOTON EMISSION OFF NUCLEONS

In this section, we describe the model for NC production of photons off nucleons,

$$\begin{aligned}\nu(k) + N(p) &\to \nu(k') + N(p') + \gamma(k_\gamma),\\ \bar{\nu}(k) + N(p) &\to \bar{\nu}(k') + N(p') + \gamma(k_\gamma).\end{aligned} \tag{1}$$

A. Kinematics and general definitions

The unpolarized differential cross section with respect to the photon kinematical variables (kinematics is sketched in Fig. 1) is given in the Laboratory (LAB) frame by

$$\frac{d^3\sigma_{(\nu,\bar{\nu})}}{dE_\gamma d\Omega(\hat{k}_\gamma)} = \frac{E_\gamma}{|\vec{k}|}\frac{G^2}{16\pi^2}\int \frac{d^3k'}{|\vec{k}'|} L^{(\nu,\bar{\nu})}_{\mu\sigma} W^{\mu\sigma}_{\mathrm{NC}\gamma}. \tag{2}$$

As we neglect the neutrino masses, $E_\nu = |\vec{k}|$, $E' = |\vec{k}'|$ and $E_\gamma = |\vec{k}_\gamma|$, where $\vec{k}$, $\vec{k}'$, and $\vec{k}_\gamma$ are the incoming neutrino, outgoing neutrino, and outgoing photon momenta in LAB, in this order; $G = 1.1664 \times 10^{-11}\ \mathrm{MeV}^{-2}$ is the Fermi constant, while $L^{(\nu,\bar{\nu})}$ and $W_{\mathrm{NC}\gamma}$ stand for the leptonic and hadronic tensors, respectively. The leptonic tensor,[1]

$$\begin{aligned}L^{(\nu,\bar{\nu})}_{\mu\sigma} &= (L_s)_{\mu\sigma} + i\left(L^{(\nu,\bar{\nu})}_a\right)_{\mu\sigma}\\ &= k'_\mu k_\sigma + k'_\sigma k_\mu + g_{\mu\sigma}\frac{q^2}{2} \pm i\epsilon_{\mu\sigma\alpha\beta}k'^\alpha k^\beta,\\ &\quad (+\to\nu, -\to\bar{\nu}),\end{aligned} \tag{3}$$

is orthogonal to the four-momentum transfer $q_\mu = k_\mu - k'_\mu$, with $q^2 = -2k\cdot k' = -4EE'\sin^2\theta'/2$. The hadronic tensor includes the nonleptonic vertices and reads

$$\begin{aligned}W^{\mu\sigma}_{\mathrm{NC}\gamma} &= \frac{1}{4M}\sum_{\text{spins}}\int \frac{d^3p'}{(2\pi)^3}\frac{1}{2E'_N}\delta^4(p' + k_\gamma - q - p)\\ &\quad\times \langle N\gamma|j^\mu_{\mathrm{NC}\gamma}(0)|N\rangle\langle N\gamma|j^\sigma_{\mathrm{NC}\gamma}(0)|N\rangle^*,\end{aligned} \tag{4}$$

with M the nucleon mass[2] and E'_N the energy of the outgoing nucleon. The bar over the sum of initial and final spins denotes the average over the initial ones. The one-particle states are normalized as $\langle\vec{p}\,|\vec{p}\,'\rangle = (2\pi)^3 2p_0\delta^3(\vec{p}-\vec{p}\,')$. Then, the matrix element $\langle N\gamma|j^\mu_{\mathrm{NC}\gamma}(0)|N\rangle$ is dimensionless. For the sake of completeness, we notice that the NC, j^μ_{NC} and electromagnetic (EM), s^μ_{EM} currents at the quark level are given by

$$\begin{aligned}j^\mu_{\mathrm{NC}} &= \bar{\Psi}_u\gamma^\mu\left(1 - \tfrac{8}{3}\sin^2\theta_W - \gamma_5\right)\Psi_u\\ &\quad - \bar{\Psi}_d\gamma^\mu\left(1 - \tfrac{4}{3}\sin^2\theta_W - \gamma_5\right)\Psi_d\\ &\quad - \bar{\Psi}_s\gamma^\mu\left(1 - \tfrac{4}{3}\sin^2\theta_W - \gamma_5\right)\Psi_s,\\ &= \bar{\Psi}_q\gamma^\mu(1-\gamma_5)\tau^{(1)}_0\Psi_q - 4\sin^2\theta_W s^\mu_{\mathrm{EM}}\\ &\quad - \bar{\Psi}_s\gamma^\mu(1-\gamma_5)\Psi_s,\end{aligned} \tag{5}$$

$$s^\mu_{\mathrm{EM}} = \tfrac{2}{3}\bar{\Psi}_u\gamma^\mu\Psi_u - \tfrac{1}{3}\bar{\Psi}_d\gamma^\mu\Psi_d - \tfrac{1}{3}\bar{\Psi}_s\gamma^\mu\Psi_s, \tag{6}$$

where Ψ_u, Ψ_d, and Ψ_s are the quark fields and θ_W the weak angle ($\sin^2\theta_W = 0.231$). The zeroth spherical component of the isovector operator $\tau^{(1)}$ is equal to the third component of the isospin Pauli matrices $\vec{\tau}$.

By construction, the hadronic tensor accomplishes

$$W^{\mu\sigma}_{\mathrm{NC}\gamma} = W^{(s)\mu\sigma}_{\mathrm{NC}\gamma} + iW^{(a)\mu\sigma}_{\mathrm{NC}\gamma}, \tag{7}$$

in terms of its real symmetric, $W^{(s)}_{\mathrm{NC}\gamma}$, and antisymmetric, $W^{(a)}_{\mathrm{NC}\gamma}$, parts. Both lepton and hadron tensors are independent of the neutrino flavor and, therefore, the cross section for the reaction of Eq. (1) is the same for electron, muon, or tau incident (anti)neutrinos.

Let us define the amputated amplitudes $\Gamma^{\mu\rho}$ as

$$\langle N\gamma|j^\mu_{\mathrm{NC}\gamma}(0)|N\rangle = \bar{u}(p')\Gamma^{\mu\rho}u(p)\epsilon^*_\rho(k_\gamma), \tag{8}$$

where the spin dependence of the Dirac spinors (normalized such that $\bar{u}u = 2M$) for the nucleons is understood, and $\epsilon(k_\gamma)$ is the polarization vector of the outgoing photon. To keep the notation simple we do not specify the type of nucleon ($N = n$ or p) in $\Gamma^{\mu\rho}$. In terms of these amputated amplitudes, and after performing the average (sum) over the initial (final) spin states, we find

$$\begin{aligned}W^{\mu\sigma}_{\mathrm{NC}\gamma} &= -\frac{1}{8M}\int\frac{d^3p'}{(2\pi)^3}\frac{1}{2E'_N}\delta^4(p' + k_\gamma - q - p)\\ &\quad\times \mathrm{Tr}\left[(\not{p}' + M)\Gamma^{\mu\rho}(\not{p} + M)\gamma^0\left(\Gamma^\sigma_{\cdot\rho}\right)^\dagger\gamma^0\right].\end{aligned} \tag{9}$$

After performing the d^3p' integration, there is still a $\delta(p'^0 + E_\gamma - q^0 - p^0)$ left in the hadronic tensor, which can be used to perform the integration over $|\vec{k}'|$ in Eq. (2).

B. Evaluation of the $\Gamma^{\mu\rho}$ amputated amplitudes

1. The $\Delta(1232)$ contribution, chiral symmetry, and nonresonant terms

Just as in pion production [35], one expects the NCγ reaction to be dominated by the excitation of the $\Delta(1232)$ supplemented with a nonresonant background. In our case, the leading nonresonant contributions are nucleon-pole terms built out of Z^0NN and γNN vertices that respect chiral symmetry. The q^2 dependence of the amplitudes is introduced via phenomenological form factors. We also take into account the subleading mechanism originated from the anomalous

[1] Our conventions are such that $\epsilon_{0123} = +1$ and $g^{\mu\nu} = (+,-,-,-)$.
[2] We take the average of the neutron and proton masses.

$Z^0\gamma\pi$ vertex, that involves a pion exchange in the t channel. Thus, in a first stage we consider the five diagrams depicted in Fig. 2. The corresponding amputated amplitudes are

$$\Gamma_N^{\mu\rho} = \Gamma_{NP}^{\mu\rho} + \Gamma_{CNP}^{\mu\rho} = ie\, J_{\rm EM}^{\rho}(-k_\gamma)\frac{\not p + \not q + M}{(p+q)^2 - M^2 + i\epsilon} J_{\rm NC}^{\mu}(q) + ie\, J_{\rm NC}^{\mu}(q)\frac{(\not p' - \not q + M)}{(p'-q)^2 - M^2 + i\epsilon} J_{\rm EM}^{\rho}(-k_\gamma), \tag{10}$$

$$\Gamma_{\pi Ex}^{\mu\rho} = eC_N \frac{g_A M}{4\pi^2 f_\pi^2}(1 - 4\sin^2\theta_W)\frac{\epsilon^{\mu\rho\sigma\alpha} q_\sigma (k_\gamma)_\alpha}{(q-k_\gamma)^2 - m_\pi^2}\gamma_5, \quad (C_N = +1 \to p, C_N = -1 \to n), \tag{11}$$

$$\Gamma_\Delta^{\mu\rho} = \Gamma_{\Delta P}^{\mu\rho} + \Gamma_{C\Delta P}^{\mu\rho} = ie\,\gamma^0 \left[J_{\rm EM}^{\alpha\rho}(p',k_\gamma)\right]^\dagger \gamma^0 \frac{P_{\alpha\beta}(p+q)}{(p+q)^2 - M_\Delta^2 + iM_\Delta\Gamma_\Delta} J_{\rm NC}^{\beta\mu}(p,q)$$
$$+ ie\,\gamma^0 \left[J_{\rm NC}^{\alpha\mu}(p', -q)\right]^\dagger \gamma^0 \frac{P_{\alpha\beta}(p'-q)}{(p'-q)^2 - M_\Delta^2 + i\epsilon} J_{\rm EM}^{\beta\rho}(p, -k_\gamma), \tag{12}$$

with $e > 0$ the electron charge, such that $\alpha = e^2/4\pi \approx 1/137$, $f_\pi = 92.4$ MeV the pion decay constant, and $g_A = 1.267$ the axial nucleon charge; m_π and $M_\Delta(\sim 1232\,\text{MeV})$ are the pion and Δ masses, respectively. As will be clear in the following, each of the building blocks of the model is gauge invariant by construction $\bar u(p')\,\Gamma^{\mu\rho}_{N,\Delta,\pi Ex}\,u(p)(k_\gamma)_\rho = 0$. The vector parts of these amplitudes are also conserved (CVC) $\bar u(p')\,V^{\mu\rho}_{N,\Delta,\pi Ex} u(p) q_\mu = 0$.

a. NP and CNP amplitudes. The nucleon NC and EM currents are given by

$$J_{\rm NC}^{\mu}(q) = \gamma^\mu \tilde F_1(q^2) + \frac{i}{2M}\sigma^{\mu\beta} q_\beta \tilde F_2(q^2) - \gamma^\mu\gamma_5 \tilde F_A(q^2), \tag{13}$$

$$J_{\rm EM}^{\mu}(k_\gamma) = \gamma^\mu F_1(0) + \frac{i}{2M}\sigma^{\mu\nu}(k_\gamma)_\nu F_2(0), \tag{14}$$

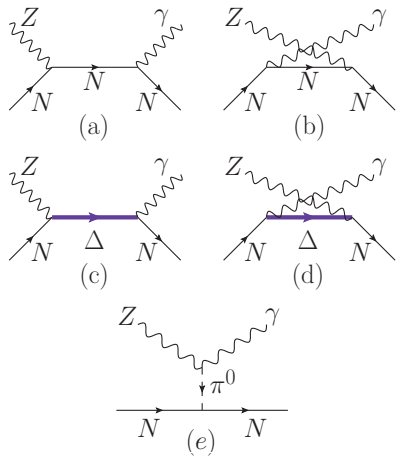

FIG. 2. (Color online) Model for photon emission off the nucleon; direct and crossed nucleon-pole terms (a) and (b), direct and crossed $\Delta(1232)$-pole terms (c) and (d), and the anomalous t-channel pion exchange term (e). Throughout this work, we denote these contributions as *NP*, *CNP*, ΔP, $C\Delta P$, and πEx, respectively.

where $\tilde F_{1,2}$ and $\tilde F_A$ are the NC vector and axial form factors[3] while $F_{1,2}$ are the EM ones. These form factors take different values for protons and neutrons. For $F_{1,2}$, we have

$$F_1^{(N)} = \frac{G_E^N + \tau G_M^N}{1+\tau}, \quad F_2^{(N)} = \frac{G_M^N - G_E^N}{1+\tau}, \quad N = p,n, \tag{15}$$

with

$$G_E^p = \frac{G_M^p}{\mu_p} = \frac{G_M^n}{\mu_n} = -(1+b\tau)\frac{G_E^n}{\mu_n a\tau} = \left(\frac{1}{1 - q^2/M_D^2}\right)^2, \tag{16}$$

where $\tau = -q^2/4M^2$, $M_D = 0.84$ GeV, $\mu_p = 2.793$, $\mu_n = -1.913$, $b = 4.61$, and $a = 0.942$ [76].

The NC vector form factors $\tilde F_{1,2}$ can be referred to the EM ones thanks to isospin symmetry relationships,

$$\tilde F_{1,2}^{(p)} = (1 - 4\sin^2\theta_W)F_{1,2}^{(p)} - F_{1,2}^{(n)} - F_{1,2}^{(s)}, \tag{17}$$

$$\tilde F_{1,2}^{(n)} = (1 - 4\sin^2\theta_W)F_{1,2}^{(n)} - F_{1,2}^{(p)} - F_{1,2}^{(s)}, \tag{18}$$

where $F_{1,2}^{(s)}$ are the strange EM form factors. Furthermore, in the axial sector one has

$$\tilde F_A^{(p,n)} = \pm F_A - F_A^{(s)}, \quad (+ \to p, - \to n), \tag{19}$$

where F_A is the axial form factor that appears in CCQE interactions, for which we adopt a conventional dipole parametrization,

$$F_A(q^2) = g_A\left(1 - \frac{q^2}{M_A^2}\right)^{-2}, \tag{20}$$

with an axial mass $M_A = 1$ GeV [77]; $F_A^{(s)}$ is the strange axial form factor. At present, the best determinations of the strange form factors are consistent with zero [78], thus they have been neglected in the present study.

[3]Note that pseudoscalar ($q^\mu\gamma_5$) terms do not contribute because $q^\mu L_{\mu\sigma}^{(\nu\bar\nu)} = 0$ when neutrino masses are neglected.

TABLE I. Properties of the resonances included in our model [86]. For each state, we list the Breit-Wigner mass (M_R), spin (J), isospin (I), parity (P), total decay width (Γ), and axial coupling [denoted $F_A(0)$ for spin 1/2 states and $C_5^A(0)$ for spin 3/2 states].

	M_R (MeV)	J	I	P	Γ (MeV)	$\Gamma(R \to N\pi)/\Gamma$	$F_A(0)$ or $C_5^A(0)$
$\Delta(1232)$	1232	3/2	3/2	+	117	100%	1.00 ± 0.11[a]
$N(1440)$	1440	1/2	1/2	+	300	65%	−0.47
$N(1520)$	1520	3/2	1/2	−	115	60%	−2.14
$N(1535)$	1535	1/2	1/2	−	150	45%	−0.21

[a]In the case of the Δ, we use a $C_5^A(0)$ value obtained in a reanalysis [36] of the $\nu_\mu p \to \mu^- p\pi^+$ ANL and BNL bubble chamber data, which is smaller than the corresponding GT relation by ∼20%.

b. πEx amplitudes. The t-channel pion exchange contribution arises from the anomalous $(\pi^0\gamma Z^0)$ Lagrangian [58],

$$\mathcal{L}_{\pi^0\gamma Z^0} = \frac{eg}{4\cos\theta_W}\frac{N_C}{12\pi^2 f_\pi}(1-4\sin^2\theta_W)\pi^0 \times \epsilon^{\mu\nu\alpha\beta}\partial_\mu Z_\nu \partial_\alpha A_\beta, \tag{21}$$

together with the leading order $\pi^0 NN$ interaction term,

$$\mathcal{L}_{\pi^0 NN} = \frac{g_A}{f_\pi}\bar{\Psi}\gamma^\mu\gamma_5\frac{\tau_3}{2}(\partial_\mu\pi^0)\Psi, \quad \Psi = \begin{pmatrix} p \\ n \end{pmatrix}, \tag{22}$$

where Ψ, π^0, A_β, Z_ν are the nucleon, neutral pion, photon, and Z^0 boson fields, respectively. In addition, $g = e/\sin\theta_W$ is related to the Fermi constant G and the W-boson mass as $G/\sqrt{2} = g^2/8M_W^2$; N_C is the number of colors. The Lagrangian of Eq. (21) arises from the Wess-Zumino-Witten term [79,80], which accounts for the axial anomaly of QCD.

c. ΔP and $C\Delta P$ amplitudes. In the Δ-driven amplitudes of Eq. (12), $P^{\mu\nu}$ is the spin 3/2 projection operator, which reads

$$P^{\mu\nu}(p_\Delta) = -(\not{p}_\Delta + M_\Delta)\Big[g^{\mu\nu} - \frac{1}{3}\gamma^\mu\gamma^\nu - \frac{2}{3}\frac{p_\Delta^\mu p_\Delta^\nu}{M_\Delta^2} + \frac{1}{3}\frac{p_\Delta^\mu\gamma^\nu - p_\Delta^\nu\gamma^\mu}{M_\Delta}\Big]; \tag{23}$$

Γ_Δ is the resonance width in its rest frame, given by

$$\Gamma_\Delta(s) = \frac{1}{6\pi}\left(\frac{f^*}{m_\pi}\right)^2\frac{M}{\sqrt{s}}\left[\frac{\lambda^{\frac{1}{2}}(s,m_\pi^2,M^2)}{2\sqrt{s}}\right]^3 \times \Theta(\sqrt{s}-M-m_\pi), \quad s = p_\Delta^2, \tag{24}$$

with $f^* = 2.14$, the $\pi N\Delta$ coupling obtained from the empirical $\Delta \to N\pi$ decay width (see Table I); $\lambda(x,y,z) = x^2+y^2+z^2-2xy-2xz-2yz$, and Θ is the step function.

The weak NC and EM currents for the nucleon to Δ transition are the same for protons or neutrons and are given by

$$\frac{1}{2}J_{\rm NC}^{\beta\mu}(p,q) = \left[\frac{\tilde{C}_3^V(q^2)}{M}(g^{\beta\mu}\not{q} - q^\beta\gamma^\mu) + \frac{\tilde{C}_4^V(q^2)}{M^2}\left(g^{\beta\mu}q\cdot p_\Delta - q^\beta p_\Delta^\mu\right) + \frac{\tilde{C}_5^V(q^2)}{M^2}(g^{\beta\mu}q\cdot p - q^\beta p^\mu)\right]\gamma_5 + \frac{\tilde{C}_3^A(q^2)}{M}(g^{\beta\mu}\not{q} - q^\beta\gamma^\mu) + \frac{\tilde{C}_4^A(q^2)}{M^2}\left(g^{\beta\mu}q\cdot p_\Delta - q^\beta p_\Delta^\mu\right) + \tilde{C}_5^A(q^2)g^{\beta\mu}, \tag{25}$$

$$J_{\rm EM}^{\beta\rho}(p,-k_\gamma) = -\left[\frac{C_3^V(0)}{M}\left(g^{\beta\rho}\not{k}_\gamma - k_\gamma^\beta\gamma^\rho\right) + \frac{C_4^V(0)}{M^2}\left(g^{\beta\rho}k_\gamma\cdot p_{\Delta c} - k_\gamma^\beta p_{\Delta c}^\rho\right) + \frac{C_5^V(0)}{M^2}\left(g^{\beta\rho}k_\gamma\cdot p - k_\gamma^\beta p^\rho\right)\right]\gamma_5, \tag{26}$$

where $p_\Delta = p+q$ and $p_{\Delta c} = p-k_\gamma$; $\tilde{C}_i^V$, $\tilde{C}_i^A$, and C_i^V are the NC vector, NC axial,[4] and EM transition form factors, respectively. As in the nucleon case, the NC vector form factors are related to the EM ones:

$$\tilde{C}_i^V(q^2) = (1-2\sin^2\theta_W)C_i^V(q^2), \tag{27}$$

according to the isovector character of the $N-\Delta$ transition. These EM form factors (and couplings) can be constrained using experimental results on pion photo and electroproduction in the Δ resonance region. In particular, they can be related to the helicity amplitudes $A_{1/2}$, $A_{3/2}$, and $S_{1/2}$ [37,81] commonly extracted in the analyses of meson electroproduction data. The explicit expressions are given in Appendix A. For the helicity amplitudes and their q^2 dependence we have taken the parametrizations of the MAID analysis [82,83].[5] In the axial sector, we adopt the Adler model [84,85]:

$$\tilde{C}_3^A(q^2) = 0, \quad \tilde{C}_4^A(q^2) = -\frac{\tilde{C}_5^A(q^2)}{4}, \tag{28}$$

[4]There is another contribution to the axial current $\tilde{C}_6^A(q^2)q^\beta q^\mu$, which does not contribute to the cross section because $q^\mu L_{\mu\sigma}^{(\nu\bar{\nu})} = 0$ for massless neutrinos.

[5]The set of $N-\Delta(1232)$ vector form factors used in [35], which were taken from Ref. [81], lead to negligible changes in the results compared to those presented below.

for the subleading (in a q^2 expansion) form factors and assume a standard dipole for the dominant,

$$\tilde{C}_5^A(q^2) = C_5^A(0)\left(1-\frac{q^2}{M_A^2}\right)^{-2}, \tag{29}$$

with $C_5^A(0) = 1.00 \pm 0.11$ and $M_A = 0.93$ GeV fixed in a fit to $\nu_\mu d \to \mu^- \Delta^{++} n$ BNL and ANL data [36].

2. The second resonance region

Here, we extend the formalism to the second resonance region, which includes three isospin 1/2 baryon resonances $P_{11}(1440)$, $D_{13}(1520)$, and $S_{11}(1535)$ (see Table I). In this way, we extend the validity of the model to higher energies. A basic problem that has to be faced with resonances is the determination of the transition form factors (coupling constants and q^2 dependence). As for the $\Delta(1232)$, we obtain vector form factors from the helicity amplitudes parametrized in Ref. [82]. The equations relating helicity amplitudes and form factors are compiled in Appendix A. Our knowledge of the axial transition form factors is much poorer. Some constraints can be imposed from PCAC and the pion-pole dominance of the pseudoscalar form factors. These allow one to derive off-diagonal Goldberger-Treiman (GT) relations between the leading axial couplings and the $N^* \to N\pi$ partial decay widths (see Table I and Appendix B for more details).

For each of the three $P_{11}(1440)$, $D_{13}(1520)$, and $S_{11}(1535)$ states, we have considered the contribution of direct (RP) and crossed (CRP) resonance pole terms as depicted in Fig. 3.

a. $N(1440)$ and $N(1535)$. The structure of the contribution of these two resonances to the amputated amplitudes is similar to the one of the nucleon [Eq. (10)]. We have

$$\begin{aligned}\Gamma_R^{\mu\rho} &= \Gamma_{RP}^{\mu\rho} + \Gamma_{CRP}^{\mu\rho} \\ &= ie\, J^{\rho}_{\mathrm{EM}(R)}(-k_\gamma)\frac{\not p + \not q + M_R}{(p+q)^2 - M_R^2 + iM_R\Gamma_R} J^{\mu}_{\mathrm{NC}(R)}(q) \\ &\quad + ie\, J^{\mu}_{\mathrm{NC}(R)}(q)\frac{(\not p' - \not q + M_R)}{(p'-q)^2 - M_R^2 + i\epsilon} J^{\rho}_{\mathrm{EM}(R)}(-k_\gamma);\end{aligned} \tag{30}$$

the resonance masses M_R are listed in Table I while the widths Γ_R are discussed in Appendix C. The EM and NC currents read

$$\begin{aligned}J^{\mu}_{\mathrm{NC}(P_{11})}(q) &= \frac{\tilde{F}_{1(P_{11})}(q^2)}{(2M)^2}(\not q q^\mu - q^2\gamma^\mu) + \frac{\tilde{F}_{2(P_{11})}(q^2)}{2M} i\sigma^{\mu\nu}q_\nu \\ &\quad + \tilde{F}_{A(P_{11})}(q^2)\gamma^\mu\gamma_5,\end{aligned} \tag{31}$$

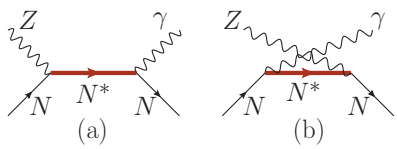

FIG. 3. (Color online) Direct (a) and crossed (b) N^* pole contributions to the NC photon emission process. We have considered the three resonances $[N(1440), N(1535), N(1520)]$ right above the $\Delta(1232)$.

$$J^{\mu}_{\mathrm{EM}(P_{11})}(k_\gamma) = \frac{F_{1(P_{11})}(0)}{(2M)^2}\not k_\gamma k_\gamma^\mu + \frac{F_{2(P_{11})}(0)}{2M} i\sigma^{\mu\nu}(k_\gamma)_\nu, \tag{32}$$

for the $N(1440)$ and

$$\begin{aligned}J^{\mu}_{\mathrm{NC}(S_{11})}(q) &= \left[\frac{\tilde{F}_{1(S_{11})}(q^2)}{(2M)^2}(\not q q^\mu - q^2\gamma^\mu) + \frac{\tilde{F}_{2(S_{11})}(q^2)}{2M} i\sigma^{\mu\nu}q_\nu\right]\gamma_5 \\ &\quad + \tilde{F}_{A(S_{11})}(q^2)\gamma^\mu,\end{aligned} \tag{33}$$

$$J^{\mu}_{\mathrm{EM}(S_{11})}(k_\gamma) = \left[\frac{F_{1(S_{11})}(0)}{(2M)^2}\not k_\gamma k_\gamma^\mu + \frac{F_{2(S_{11})}(0)}{2M} i\sigma^{\mu\nu}(k_\gamma)_\nu\right]\gamma_5 \tag{34}$$

for the $N(1535)$.[6] As in the nucleon case, isospin symmetry implies that

$$\begin{aligned}\tilde{F}^{(p)}_{1,2(R)} &= (1-4\sin^2\theta_W)F^{(p)}_{1,2(R)} - F^{(n)}_{1,2(R)} - F^{(s)}_{1,2(R)}, \\ \tilde{F}^{(n)}_{1,2(R)} &= (1-4\sin^2\theta_W)F^{(n)}_{1,2(R)} - F^{(p)}_{1,2(R)} - F^{(s)}_{1,2(R)},\end{aligned} \tag{35}$$

with $F^{(N)}_{1,2(P_{11},S_{11})}$ expressed in terms of the corresponding helicity amplitudes (see Appendix A). The NC axial form factors are

$$\begin{aligned}\tilde{F}^{(p,n)}_{A(R)} &= \pm F_{A(R)} + F^s_{A(R)}, \quad (+\to p, -\to n) \\ F_{A(R)}(q^2) &= F_{A(R)}(0)\left(1-\frac{q^2}{M_A^{*2}}\right)^{-2}.\end{aligned} \tag{36}$$

The couplings $F_{A(P_{11},S_{11})}(0)$ are obtained from the GT corresponding relations and have values given in Table I. The q^2 dependence of these form factors is unknown so we have assumed a dipole ansatz with a natural value of $M_A^* = 1.0$ GeV for the axial mass. No information is available about the strange form factors $F^{(s)}_{1,2,A(P_{11},S_{11})}$ but they are likely to be small and to have a negligible impact on the observables, so we set them to zero.

b. $N(1520)$. In this case, the structure of the contribution of this resonance to the amputated amplitudes is similar to that of the $\Delta(1232)$, differing just in the definition of the appropriate form factors and the isospin dependence. Thus, we have

$$\begin{aligned}\Gamma^{\mu\rho}_{D_{13}} &= \Gamma^{\mu\rho}_{D_{13}P} + \Gamma^{\mu\rho}_{CD_{13}P} \\ &= ie\,\gamma^0\left[J^{\alpha\rho}_{\mathrm{EM}(D_{13})}(p',k_\gamma)\right]^\dagger\gamma^0 \\ &\quad \times \frac{P^{D_{13}}_{\alpha\beta}(p+q)}{(p+q)^2 - M^2_{D_{13}} + iM_{D_{13}}\Gamma_{D_{13}}} J^{\beta\mu}_{\mathrm{NC}(D_{13})}(p,q) \\ &\quad + ie\,\gamma^0\left[J^{\alpha\mu}_{\mathrm{NC}(D_{13})}(p',-q)\right]^\dagger\gamma^0 \\ &\quad \times \frac{P^{D_{13}}_{\alpha\beta}(p'-q)}{(p'-q)^2 - M^2_{D_{13}} + i\epsilon} J^{\beta\rho}_{\mathrm{EM}(D_{13})}(p,-k_\gamma),\end{aligned} \tag{37}$$

[6]Note that by construction gauge invariance and CVC are satisfied. This is also the case for the $N(1520)$ amplitudes that will be discussed next.

where the resonance mass $M_{D_{13}}$ is given in Table I and the width $\Gamma_{D_{13}}$ is discussed in Appendix C; $P^{D_{13}}_{\mu\nu}$ is the spin 3/2 projection operator given also by Eq. (23), with the obvious replacement of M_Δ by $M_{D_{13}}$. In addition, the $N - N(1520)$ EM and NC transition currents are given by

$$J^{\beta\mu}_{\mathrm{NC}(D_{13})}(p,q) = \frac{\tilde{C}^V_{3(D_{13})}(q^2)}{M}(g^{\beta\mu}\not{q} - q^\beta\gamma^\mu) + \frac{\tilde{C}^V_{4(D_{13})}(q^2)}{M^2}\left(g^{\beta\mu}q\cdot p_{D_{13}} - q^\beta p^\mu_{D_{13}}\right) + \frac{\tilde{C}^V_{5(D_{13})}(q^2)}{M^2}(g^{\beta\mu}q\cdot p - q^\beta p^\mu) + \left[\frac{\tilde{C}^A_{3(D_{13})}(q^2)}{M}(g^{\beta\mu}\not{q} - q^\beta\gamma^\mu) + \frac{\tilde{C}^A_{4(D_{13})}(q^2)}{M^2}\left(g^{\beta\mu}q\cdot p_{D_{13}} - q^\beta p^\mu_{D_{13}}\right) + \tilde{C}^A_{5(D_{13})}(q^2)g^{\beta\mu}\right]\gamma_5, \tag{38}$$

$$J^{\beta\rho}_{\mathrm{EM}(D_{13})}(p,-k_\gamma) = -\left[\frac{C^V_{3(D_{13})}(0)}{M}\left(g^{\beta\rho}\not{k}_\gamma - k^\beta_\gamma\gamma^\rho\right) + \frac{C^V_{4(D_{13})}(0)}{M^2}\left(g^{\beta\rho}k_\gamma\cdot p_{D_{13}c} - k^\beta_\gamma p^\rho_{D_{13}c}\right) + \frac{C^V_{5(D_{13})}(0)}{M^2}\left(g^{\beta\rho}k_\gamma\cdot p - k^\beta_\gamma p^\rho\right)\right], \tag{39}$$

where $p_{D_{13}} = p + q$ and $p_{D_{13}c} = p - k_\gamma$; $\tilde{C}^V_{i(D_{13})}$, $\tilde{C}^A_{i(D_{13})}$, and $C^V_{i(D_{13})}$ are the NC vector, NC axial, and EM form factors, respectively. The NC vector form factors are related to the EM ones in the same way as for the other isospin 1/2 states considered above, namely,

$$\begin{aligned}\tilde{C}^{V(p)}_{i(D_{13})} &= (1 - 4\sin^2\theta_W)C^{(p)}_{i(D_{13})} - C^{(n)}_{i(D_{13})} - C^{(s)}_{i(D_{13})},\\ \tilde{C}^{V(n)}_{i(D_{13})} &= (1 - 4\sin^2\theta_W)C^{(n)}_{i(D_{13})} - C^{(p)}_{i(D_{13})} - C^{(s)}_{i(D_{13})},\end{aligned} \tag{40}$$

where $C^{(p,n)}_{3-5(D_{13})}$ are obtained from the helicity amplitudes using Eqs. (A14)–(A16). For the axial form factors, one again has that

$$\tilde{C}^{A(p,n)}_{i(D_{13})} = \pm C^A_{i(D_{13})} + C^{sA}_{i(D_{13})}, \quad (+\to p, -\to n). \tag{41}$$

We take a standard dipole form for the dominant axial NC form factor,

$$C^A_{5(D_{13})}(q^2) = C^A_{5(D_{13})}(0)\left(1 - \frac{q^2}{M^{*2}_A}\right)^{-2}, \tag{42}$$

with $C^A_{5(D_{13})}(0)$ from the corresponding off-diagonal GT relation (see Appendix B and Table I), and set $M^*_A = 1.0$ GeV as for the other N^*. The other axial form factors $C^A_{3,4(D_{13})}$ are less important because their contribution to the amplitude squared is proportional to q^2. We neglect them together with the unknown strange vector and axial form factors.

III. NEUTRAL-CURRENT PHOTON EMISSION IN NUCLEI

In this section we outline the framework followed to describe NC photon emission off nuclei. Both incoherent and coherent reaction channels are considered.

A. Incoherent neutral-current photon emission

To study the incoherent reactions,

$$\begin{aligned}\nu_l(k) + A_Z &\to \nu_l(k') + \gamma(k_\gamma) + X,\\ \bar{\nu}_l(k) + A_Z &\to \bar{\nu}_l(k') + \gamma(k_\gamma) + X,\end{aligned} \tag{43}$$

we pursue the many-body scheme derived in Refs. [20,30,87] for the neutrino propagation in nuclear matter and adapted to (semi)inclusive reactions on finite nuclei by means of the local density approximation. With this formalism, the photon emission cross section is

$$\sigma_{(\nu,\bar{\nu})}|_{\mathrm{incoh}} = \frac{1}{|\vec{k}|}\frac{G^2}{16\pi^2}\int\frac{d^3k'}{|\vec{k}'|}L^{(\nu,\bar{\nu})}_{\mu\sigma}W^{\mu\sigma}_{\mathrm{NC}\gamma}\Big|_{\mathrm{incoh}}, \tag{44}$$

in terms of the leptonic tensor of Eq. (3) and the hadronic tensor $W^{\mu\sigma}_{\mathrm{NC}\gamma}|_{\mathrm{incoh}} = W^{(s)\mu\sigma}_{\mathrm{NC}\gamma}|_{\mathrm{incoh}} + iW^{(a)\mu\sigma}_{\mathrm{NC}\gamma}|_{\mathrm{incoh}}$, which is determined by the contributions to the Z^0 self-energy with a photon in the intermediate state $\Pi^{\mu\sigma}_{Z\gamma}(q)$,

$$W^{(s)\mu\sigma}_{\mathrm{NC}\gamma}|_{\mathrm{incoh}} = -\Theta(q^0)\left(\frac{4\cos\theta_W}{g}\right)^2 \times\int\frac{d^3r}{2\pi}\mathrm{Im}\left[\Pi^{\mu\sigma}_{Z\gamma} + \Pi^{\sigma\mu}_{Z\gamma}\right](q,r), \tag{45}$$

$$W^{(a)\mu\sigma}_{\mathrm{NC}\gamma}|_{\mathrm{incoh}} = -\Theta(q^0)\left(\frac{4\cos\theta_W}{g}\right)^2 \times\int\frac{d^3r}{2\pi}\mathrm{Re}\left[\Pi^{\mu\sigma}_{Z\gamma} - \Pi^{\sigma\mu}_{Z\gamma}\right](q,r). \tag{46}$$

In the density expansion proposed in Ref. [20], the lowest order contribution to $\Pi^{\mu\sigma}_{Z\gamma}$ is depicted in Fig. 4. The black dots stand for any of the 11 terms [NP, CNP, πEx, RP, CRP with $R = \Delta(1232)$, $N(1440)$, $N(1520)$, $N(1535)$] of the elementary $Z^0N \to \gamma N$ amplitude derived in Sec. II. The solid upwards and downwards oriented lines represent nucleon particle and hole states in the Fermi sea. This Z^0 self-energy diagram (actually 121 diagrams) is readily evaluated as[7]

$$\begin{aligned}-i\Pi^{\mu\nu}_{Z\gamma;1p1h\gamma}(q,r) &= i\left(\frac{g}{4\cos\theta_W}\right)^2\sum_{N=p,n}\int\frac{d^4k_\gamma}{(2\pi)^4}\int\frac{d^4p}{(2\pi)^4}\frac{1}{k^2_\gamma + i\epsilon}\\ &\times\mathrm{Tr}\left[S(p,\rho_N)\gamma^0\left(\Gamma^{\mu\rho}_N\right)^\dagger\gamma^0 S(p',\rho_N)(\Gamma_N)^\nu_{\cdot\rho}\right],\end{aligned} \tag{47}$$

[7] In Eq. (47), it is necessary to subtract the free space contribution, i.e., the one that survives for vanishing nuclear densities and renormalizes free space couplings and masses. Actually, to obtain Eq. (52), we have neglected the contribution of the antiparticle pole [$p^0 = -E(\vec{p}) - i\epsilon$] in the p^0 integration. This automatically removes the unwanted vacuum part.

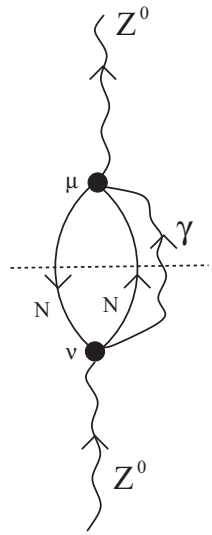

FIG. 4. Diagrammatic representation of the one-particle-one-hole-photon (1p1hγ) contributions to the Z^0 self-energy in nuclear matter. The black dots represent $Z^0N \to \gamma N$ amplitudes.

where $p' = p + q - k_\gamma$ and $\Gamma_N^{\mu\rho}$ is the amputated amplitude for the $Z^0N \to N\gamma$ process

$$\Gamma_N^{\mu\rho} = \sum_a \Gamma_{a;N}^{\mu\rho},$$
$$a = NP, CNP, \pi Ex, RP, CRP$$
$$[R = \Delta(1232), N(1440), N(1520), N(1535)]. \quad (48)$$

The nucleon propagator in the medium reads

$$S(p,\rho_N) = (\not{p} + M)G(p,\rho_N), \quad (49)$$

with

$$G(p\,;\rho_N) = \frac{1}{p^2 - M^2 + i\epsilon} + i\frac{\pi}{E(\vec{p}\,)} n_N(\vec{p}\,)\delta(p^0 - E(\vec{p}\,)) \quad (50)$$

$$= \frac{1}{p^0 + E(\vec{p}\,) + i\epsilon} \times \left(\frac{n_N(\vec{p}\,)}{p^0 - E(\vec{p}\,) - i\epsilon} + \frac{1 - n_N(\vec{p}\,)}{p^0 - E(\vec{p}\,) + i\epsilon}\right). \quad (51)$$

The occupation number in the local Fermi gas $n_N(\vec{p}\,) = \Theta(k_F^N - |\vec{p}\,|)$ depends on the local density of nucleons (protons or neutrons) in the nucleus via $k_F^N(r) = (3\pi^2\rho_N(r))^{1/3}$. The nucleon energy $E(\vec{p})$ is approximated by the free one $\sqrt{\vec{p}^{\,2} + M^2}$. Substituting the explicit expressions of $S(p,\rho_N)$ and $S(p',\rho_N)$ in Eq. (47) one obtains

$$-i\Pi_{Z\gamma;1p1h\gamma}^{\mu\nu}(q,r) = -\left(\frac{g}{4\cos\theta_W}\right)^2 \sum_{N=p,n} \int \frac{d^4k_\gamma}{(2\pi)^4} \int \frac{d^3p}{(2\pi)^3} \frac{1}{2E(\vec{p}\,)} \frac{1}{2E(\vec{p}+\vec{q}-\vec{k}_\gamma)} \frac{n_N(\vec{p}\,)[1 - n_N(\vec{p}+\vec{q}-\vec{k}_\gamma)]}{q^0 - k_\gamma^0 + E(\vec{p}\,) - E(\vec{p}\,') + i\epsilon}$$
$$\times \frac{1}{k_\gamma^2 + i\epsilon} \mathrm{Tr}\left[(\not{p} + M)\gamma^0 \left(\Gamma_N^{\mu\rho}\right)^\dagger \gamma^0 (\not{p}' + M)(\Gamma_N)^\nu_{\cdot\rho}\right] + [(q - k_\gamma) \leftrightarrow -(q - k_\gamma)]. \quad (52)$$

A convenient simplification can be made by evaluating the $\Gamma_N^{\mu\rho}$ amplitudes at an average nucleon hole four-momentum $\langle p^\mu \rangle$. This allows us to take the spin trace in Eq. (52) out of the d^3p integration, which gives, up to constants, the Lindhard function, $\overline{U}_R(q - k_\gamma, k_F^N, k_F^N)$ (see Appendix B of Ref. [20] for definition and explicit expressions). Therefore,

$$-i\Pi_{Z\gamma;1p1h\gamma}^{\mu\nu}(q,r) = -\left(\frac{g}{4\cos\theta_W}\right)^2 \frac{1}{4M^2} \sum_{N=p,n} \int \frac{d^4k_\gamma}{(2\pi)^4} \frac{1}{k_\gamma^2 + i\epsilon} \overline{U}_R\left(q - k_\gamma, k_F^N, k_F^N\right) A_N^{\mu\nu}(\langle p\rangle, q, k_\gamma), \quad (53)$$

$$A_N^{\mu\nu} = \frac{1}{2}\mathrm{Tr}\left[(\langle\not{p}\rangle + M)\gamma^0(\langle\Gamma_N\rangle^{\mu\rho})^\dagger\gamma^0(\langle\not{p}\rangle + \not{q} - \not{k}_\gamma + M)\langle\Gamma_N\rangle^\nu_{\cdot\rho}\right], \quad (54)$$

where $\langle\Gamma_N\rangle^{\nu\rho}$ stands for $\Gamma_N^{\nu\rho}$ calculated at the average hole four-momentum $\langle p^\mu\rangle$.

To derive the 1p1hγ contribution to the hadron tensor $W^{\mu\sigma}$, we remind that by construction,

$$A_N^{\mu\nu} = A_N^{(s)\mu\nu} + iA_N^{(a)\mu\nu}, \quad (55)$$

where $A_N^{(s)\mu\sigma}$ ($A_N^{(a)\mu\sigma}$) is a real symmetric (antisymmetric) tensor. Furthermore, it is easy to see that the combinations of the Z^0 self-energy present in Eqs. (45) and (46) fulfill

$$\mathrm{Im}\left[\Pi_{Z\gamma;1p1h\gamma}^{\mu\nu} + \Pi_{Z\gamma;1p1h\gamma}^{\nu\mu}\right] = 2\mathrm{Im}\Pi_{Z\gamma;1p1h\gamma}^{(s)\mu\nu},$$
$$\mathrm{Re}\left[\Pi_{Z\gamma;1p1h\gamma}^{\mu\nu} - \Pi_{Z\gamma;1p1h\gamma}^{\nu\mu}\right] = -2\mathrm{Im}\Pi_{Z\gamma;1p1h\gamma}^{(a)\mu\nu}, \quad (56)$$

where $\Pi_{Z\gamma;1p1h\gamma}^{(s,a)\mu\nu}$ are obtained by replacing $A_N^{\mu\nu}$ in Eq. (53) by the corresponding $A_N^{(s,a)\mu\nu}$ parts.

The imaginary part of $\Pi_{ZW;1p1h\gamma}^{\mu\nu}|_{s(a)}$ can be obtained following the Cutkosky rules. In this case we cut the self-energy diagram of Fig. 4 with a straight horizontal line. The states intercepted by the line are placed on shell by taking the imaginary part of their propagators. Technically, the rules to obtain $\mathrm{Im}\Pi_{Z;1p1h\gamma}^{\mu\nu}$ consist of the following substitutions:

$$\Pi_{Z\gamma}^{\mu\nu}(q) \to 2i\mathrm{Im}\Pi_{Z\gamma}^{\mu\nu}(q)\Theta(q^0), \quad (57)$$

$$\frac{1}{k_\gamma^2 + i\epsilon} \to 2i\mathrm{Im}\frac{1}{k_\gamma^2 + i\epsilon}\Theta\left(k_\gamma^0\right) = -2\pi i\delta(k_\gamma^2)\Theta\left(k_\gamma^0\right), \quad (58)$$

$$\overline{U}_R\left(q-k_\gamma,k_F^N,k_F^N\right)\to 2i\,\mathrm{Im}\overline{U}_R\left(q-k_\gamma,k_F^N,k_F^N\right)\Theta\left(q^0-k_\gamma^0\right). \tag{59}$$

Thus, taking into account that $A_N^{(s,a)\mu\nu}$ are real, we readily obtain

$$W_{1p1h\gamma}^{\mu\nu}(q)=\Theta(q^0)\frac{1}{2M^2}\int\frac{d^3r}{2\pi}\sum_{N=p,n}\frac{d^3k_\gamma}{(2\pi)^3}\frac{\Theta(q^0-E_\gamma)}{2E_\gamma}\times\mathrm{Im}\overline{U}_R\left(q-k_\gamma,k_F^N,k_F^N\right)A_N^{\nu\mu}, \tag{60}$$

with E_γ the photon on-shell energy.

The average nucleon hole momentum $\langle p^\mu\rangle$ is chosen as follows [see the discussion after Eq. (9) of Ref. [39]]:

$$\langle p^0\rangle=\frac{E_F^N+E_{\min}}{2},\quad \langle|\vec{p}\,|\rangle=\sqrt{\langle p^0\rangle^2-M^2}, \tag{61}$$

defined by the central value of the allowed energy region, with

$$E_{\min}=\max\left(M,E_F^N-q'^0,\frac{-q'^0+|\vec{q}\,'|\sqrt{1-4M^2/q'^2}}{2}\right), \tag{62}$$

where $q'=q-k_\gamma$ and $E_F^N=\sqrt{M^2+(k_F^N)^2}$. The corresponding nucleon hole angle, in the LAB frame and with respect to $\vec{q}\,'$, is completely fixed by the kinematics to

$$\cos\theta_N=\frac{q'^2+2\langle p^0\rangle q'^0}{2\langle|\vec{p}\,|\rangle|\vec{q}\,'|}, \tag{63}$$

while the azimuthal angle ϕ_N is fixed arbitrarily in the plane perpendicular to $\vec{q}\,'$. Similar approximations were performed, and shown to be sufficiently accurate, in studies of total inclusive and pion production in photo and electronuclear reactions [71–73,88]. They were also used in Ref. [30] to compute the total inclusive neutrino-induced cross section. We have checked that the approximation of Eqs. (61)–(63) induces uncertainties of at most 5%, independently of ϕ_N values. Furthermore, different choices of ϕ_N produce small variations of the order of 1%–2% in the results. This approximation saves a considerable amount of computational time because there are analytical expressions for $\mathrm{Im}\overline{U}_R(q-k_\gamma,k_F^N,k_F^N)$ (see, for instance, Ref. [20]).

In the small density limit $\mathrm{Im}\overline{U}_R(q',k_F^N,k_F^N)\simeq -\pi\rho_N M\delta(q'^0+M-\sqrt{M^2+\vec{q}\,'^2})/\sqrt{M^2+\vec{q}\,'^2}$. Substituting this expression in Eq. (60) one obtains

$$\lim_{\rho\to 0}W_{1p1h\gamma}^{\mu\nu}\sim\int d\Omega(\hat{k}_\gamma)dE_\gamma E_\gamma\left(ZW_{Z^0p\to p\gamma}^{\mu\nu}+NW_{Z^0n\to n\gamma}^{\mu\nu}\right), \tag{64}$$

where Z and N are the number of protons and neutrons in the nucleus, and $W_{Z^0N\to N\gamma}^{\mu\nu}$ is the hadronic tensor for NC photon production on the nucleon. In this way, the strict impulse approximation is recovered. By performing the integral in Eq. (60), Pauli blocking and Fermi motion are taken into account.

1. Further nuclear medium corrections

Given the dominant role played by the ΔP contribution and because Δ properties are strongly modified in the nuclear medium [69,89–94] a proper treatment of the Δ contribution is needed. Here, we follow Ref. [45] and modify the Δ propagator in the ΔP term as

$$\frac{1}{p_\Delta^2-M_\Delta^2+iM_\Delta\Gamma_\Delta}\to\frac{1}{\sqrt{p_\Delta^2}+M_\Delta}\frac{1}{\sqrt{p_\Delta^2}-M_\Delta+i\left(\Gamma_\Delta^{\mathrm{Pauli}}/2-\mathrm{Im}\Sigma_\Delta\right)}; \tag{65}$$

$\Gamma_\Delta^{\mathrm{Pauli}}$, for which we take the expression in Eq. (15) of Ref. [70], is the free Δ width corrected by the Pauli blocking of the final nucleon. The imaginary part of the Δ self-energy in the medium $\mathrm{Im}\Sigma_\Delta$, is parametrized as [91]

$$-\mathrm{Im}\Sigma_\Delta(\rho)=C_Q\left(\frac{\rho}{\rho_0}\right)^\alpha+C_{A2}\left(\frac{\rho}{\rho_0}\right)^\beta+C_{A3}\left(\frac{\rho}{\rho_0}\right)^\gamma, \tag{66}$$

where the term proportional to C_Q accounts for the QE part while those with coefficients C_{A2} and C_{A3} correspond to the two-body ($\Delta N\to NN$) and three-body ($\Delta NN\to NNN$) absorption contributions, respectively. The parameters in Eq. (66) can be found in Eq. (4.5) and Table II of Ref. [91], given as functions of the kinetic energy in the laboratory system of a pion that would excite a Δ with the corresponding invariant mass. These parametrizations are valid in the range 85 MeV $< T_\pi <$ 315 MeV. Below 85 MeV, the contributions from C_Q and C_{A3} are rather small and are taken from Ref. [70], where the model was extended to low energies. The term with C_{A2} shows a very mild energy dependence and we still use the parametrization from Ref. [91] even at low energies. For T_π above 315 MeV we have kept these self-energy terms constant and equal to their values at the bound. The uncertainties in these pieces are not very relevant there because the $\Delta\to N\pi$ decay becomes very large and absolutely dominant.

For the Δ mass we shall keep its free value. While there are some corrections arising from both the real part of the self-energy and random phase approximation (RPA) sums, the net effect is smaller than the precision achievable in current neutrino experiments, and also smaller than the uncertainties due to our limited knowledge of the nucleon to Δ transition form factor $C_5^A(q^2)$ (see the related discussion in Sec. IIE of Ref. [30]).

B. Coherent neutral-current photon emission

The coherent reactions,

$$\begin{aligned}\nu_l(k)+A_Z|_{gs}(p_A)&\to\nu_l(k')+A_Z|_{gs}(p'_A)+\gamma(k_\gamma),\\ \bar{\nu}_l(k)+A_Z|_{gs}(p_A)&\to\bar{\nu}_l(k')+A_Z|_{gs}(p'_A)+\gamma(k_\gamma),\end{aligned} \tag{67}$$

consist of a weak photon production where the nucleus is left in its ground state, in contrast with the incoherent production that we studied in the previous subsection, where the nucleus is either broken or left in an excited state. Here, we adopt the

framework derived in Ref. [46] for neutrino-induced coherent CC and NC pion production reactions.[8] This work is, in turn, based on previous studies of coherent pion production in electromagnetic [(γ,π^0) [74], $(e,e'\pi^0)$ [75]] and hadronic reactions [$(^3\mathrm{He},^3\mathrm{H}\,\pi^+)$ [96], $p(^4\mathrm{He},^4\mathrm{He})X$ [97]] in the $\Delta(1232)$ region. More recently, the same scheme was employed to study charged kaon production by coherent scattering of neutrinos and antineutrinos on nuclei [98]. The model for the coherent process is built up from the coherent scattering with each of the nucleons of the nucleus, producing an outgoing γ. The nucleon state (wave function) remains unchanged so that after summing over all nucleons, one obtains the nuclear densities. In the elementary $Z^0N \to N\gamma$ process, energy conservation is accomplished by imposing $q^0 = E_\gamma$, which is justified by the large nucleus mass, while the transferred momentum $\vec{q} - \vec{k}_\gamma$ has to be accommodated by the nucleon wave functions. Therefore, the coherent production process is sensitive to the Fourier transform of the nuclear density.

Following Ref. [46], it is straightforward to find that

$$\left.\frac{d^3\sigma_{(\nu,\bar\nu)}}{dE_\gamma d\Omega(\hat{k}_\gamma)}\right|_{\rm coh} = \frac{E_\gamma}{|\vec{k}|}\frac{G^2}{16\pi^2}\int\frac{d^3k'}{|\vec{k}'|}L^{(\nu,\bar\nu)}_{\mu\sigma}W^{\mu\sigma}_{\mathrm{NC}\gamma}\big|_{\rm coh}, \tag{68}$$

$$W^{\mu\sigma}_{\mathrm{NC}\gamma}\big|_{\rm coh} = -\frac{\delta(E_\gamma - q^0)}{64\pi^3M^2}\mathcal{A}^{\mu\rho}(q,k_\gamma)\left(\mathcal{A}^{\sigma}_{\ \rho}(q,k_\gamma)\right)^*, \tag{69}$$

$$\mathcal{A}^{\mu\rho}(q,k_\gamma) = \int d^3r\; e^{i(\vec{q}-\vec{k}_\gamma)\cdot\vec{r}}\left\{\rho_p(r)\hat{\Gamma}^{\mu\rho}_p(r;q,k_\gamma) + \rho_n(r)\hat{\Gamma}^{\mu\rho}_n(r;q,k_\gamma)\right\}. \tag{70}$$

To evaluate the hadronic tensor, we use the model for the NC photon production off the nucleon derived in Sec. II and thus we have

$$\hat{\Gamma}^{\mu\rho}_N(r;q,k_\gamma) = \sum_i \hat{\Gamma}^{\mu\rho}_{i;N}(r;q,k_\gamma),$$
$$i = NP, CNP, \pi Ex, RP, CRP$$
$$[R = \Delta, N(1440), N(1535), N(1520)], \tag{71}$$

$$\hat{\Gamma}^{\mu\rho}_{i;N}(r;q,k_\gamma) = \frac{1}{2}\mathrm{Tr}\left[(\not{p}+M)\gamma^0\,\Gamma^{\mu\rho}_{i;N}\right] \times\left.\frac{M}{p^0}\right|_{p^\mu=\left(\sqrt{M^2+\frac{(\vec{k}_\gamma-\vec{q})^2}{4}},\frac{1}{2}(\vec{k}_\gamma-\vec{q})\right)}, \tag{72}$$

where the four-vector matrices $\Gamma^{\mu\rho}_{i;N\gamma}$ stand for the amputated photon production amplitudes off nucleons derived in Sec. II B. We have also taken into account the modification of the $\Delta(1232)$ in the medium for the ΔP mechanism, as explained in Sec. III A 1.

Now we pay attention to the approximated treatment of nucleon momentum distributions that has been adopted to obtain Eqs. (69)–(72). The initial ($\vec{p}$) and final ($\vec{p}\,'$) nucleon three momenta are not well defined. We take

$$p^\mu = \left(\sqrt{M^2+\frac{1}{4}(\vec{k}_\gamma-\vec{q})^2}, \frac{\vec{k}_\gamma-\vec{q}}{2}\right),$$
$$p'^\mu = q - k_\gamma + p = \left(\sqrt{M^2+\frac{1}{4}(\vec{k}_\gamma-\vec{q})^2}, -\frac{\vec{k}_\gamma-\vec{q}}{2}\right), \tag{73}$$

with both nucleons being on-shell. In this way, the momentum transfer is equally shared between the initial and final nucleons. This prescription, employed in Refs. [45,46,48,68], for (anti)neutrino-induced coherent pion production, was earlier applied to $^{16}\mathrm{O}(\gamma,\pi^+)^{16}\mathrm{N}_{\rm bound}$ [99] and to coherent π^0 photo- and electroproduction [74,75,100]. The approximation is based on the fact that, for Gaussian nuclear wave functions, it leads to an exact treatment of the terms in the elementary amplitude that are linear in momentum. In Ref. [74] it was shown that in the case of π^0 photoproduction, this prescription provided similar results as the explicit sum over the nucleon momenta performed in Ref. [101]. Thanks to the choice of Eq. (73), the sum over all nucleons is greatly simplified and cast in terms of the neutron and proton densities [see Eq. (70)]. Furthermore, the sum over nucleon helicities gives rise to the trace in Eq. (72); more details can be found in the discussion after Eq. (6) of Ref. [46]. On the other hand, this approximation eliminates some nonlocal contributions to the amplitudes. In particular, the Δ momentum turns out to be well defined once the nucleon momenta are fixed. In Ref. [102] this constraint was relaxed for weak coherent pion production via $\Delta(1232)$ excitation, while neglecting the modification of the Δ properties in the nucleus and pion distortion. It was found that nonlocalities in the Δ propagation cause a large reduction of the cross section at low energies. In the more realistic description of Nakamura *et al.* [47], the nonlocality is preserved for the Δ kinetic term in a linearized version of the Δ propagator but, at the same time, a prescription similar to Eq. (73) for the $WN\Delta$ and $\Delta N\pi$ vertices, and a local ansatz for the in-medium Δ self-energy have been taken. Nevertheless, the mismatch between the nonlocal recoil effects and the local approximations for vertices and self-energy are likely to be minimized by the fact that the parameters in the Δ self-energy are adjusted to describe pion-nucleus scattering data with the same model. Our point of view is that the local approach adopted here and in Refs. [45,46,48,68], together with the choice of the effective nucleon-nucleon interaction in the medium [91], is internally consistent. The good agreement obtained for pion-nucleus scattering [70,103] and coherent pion photoproduction [48,104] for medium and heavy nuclei seems to support this conjecture, although more detailed investigations are necessary. In any case, for the present study, where the coherent contribution is a small and not disentangled part of the total NCγ cross section, and in view of the uncertainty in the determination of the $N\Delta$ axial coupling $C_5^A(0)$, it is safe to disregard possible nonlocal corrections.

[8]The predictions of Ref. [46] were updated in [95] after the reanalysis of the $\nu_\mu p \to \mu^- p\pi^+$ old bubble chamber data carried out in Ref. [36].

IV. RESULTS

Before discussing our results an important remark is due. The intermediate nucleon propagators in both the *NP* and *CNP* terms of Eq. (10) can be put on the mass shell for $E_\gamma \to 0$ photons, leading to an infrared divergence. This divergence should be canceled by others present in the electromagnetic radiative corrections to the elastic process $\nu N \to \nu N$ (without photon emission). However, when the emitted photon is too soft, its energy becomes smaller than the photon energy resolution of the detector. Such an event would be recorded as an elastic one if at all. For this reason, we have implemented a cut in the available photon phase space, demanding $E_\gamma \geqslant 140$ MeV, which corresponds to the MiniBooNE detection threshold [56].

A. Neutral-current photon emission off nucleons

In Fig. 5, we show our results for the total NC photon emission (anti)neutrino cross sections as a function of the (anti)neutrino energy. As in other weak interaction processes, the different helicities of ν and $\bar{\nu}$ are responsible for different interference patterns, resulting in smaller $\bar{\nu}$ cross sections with a more linear energy dependence. The error bands on the full model results are determined by the uncertainty in the axial $N\Delta$ coupling $C_5^A(0) = 1.00 \pm 0.11$ [36]. This is the predominant source of uncertainty in the (anti)neutrino energy range under consideration (see also the discussion of Fig. 8 below). We also display the contributions from the different mechanisms considered in our model (Figs. 2 and 3). The Δ mechanism is dominant and gives the same contribution for protons and neutrons, as expected from the isovector nature of the electroweak $N - \Delta$ transition. At $E_{\nu(\bar{\nu})} \sim 1.5$ GeV, the cross section from nucleon-pole terms is only about 2.5 smaller than the Δ one. Above ~1.5 GeV, the $N(1520)$ contribution is sizable and comparable to that of the sum of the *NP* and *CNP* mechanisms, specially for $\bar{\nu}p$. However, the rest of the N^* contributions considered in the model [with $N(1440)$ and $N(1535)$ intermediate states], together with the πEx contribution of Fig. 2(e) can be safely neglected in the whole range of (anti)neutrino energies considered in this work. The fact that the $N(1520)$ resonance is the only one, in addition to the $\Delta(1232)$, playing a significant role for $E_\nu < 2$ GeV was also observed in pion production [39] and for the inclusive cross section [37].

Photon angular and energy distributions on single nucleons, for incoming (anti)neutrino energies of 1 and 2 GeV are shown in Figs. 6 and 7. Solid curves stand for the results from the full model. We also display the largest contributions among the different mechanisms considered in our model. As expected, the Δ mechanisms are also dominant in the differential cross sections, especially for reactions on neutrons and even more so for the $\bar{\nu}n \to \bar{\nu}n\gamma$ process. Nucleon and D_{13} direct and crossed pole-term contributions, though small, are not negligible, particularly for protons. The $N(1520)$ terms become more important for the largest (anti)neutrino energy.

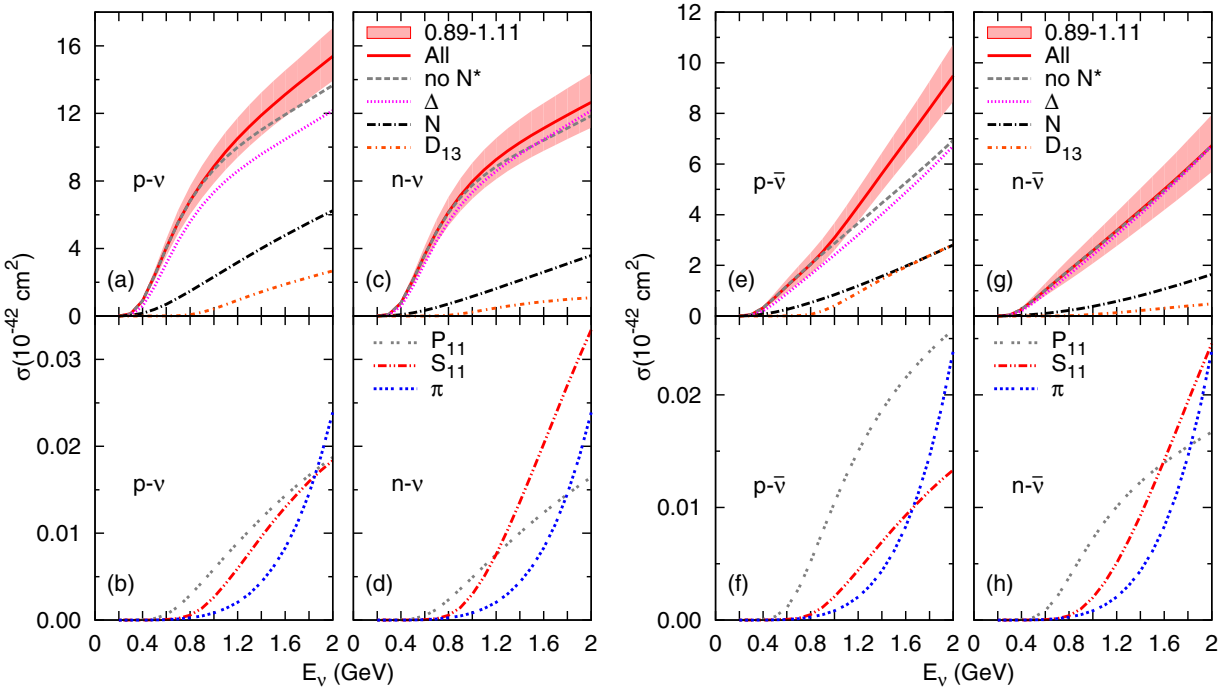

FIG. 5. (Color online) $\nu N \to \nu N\gamma$ (left) and $\bar{\nu}N \to \bar{\nu}N\gamma$ (right) cross sections on protons and neutrons as a function of the (anti)neutrino energy. A cut of $E_\gamma \geqslant 140$ MeV in the phase space integrals was applied. Solid curves correspond to the results from the full model, with error bands determined by the uncertainty in the axial $N\Delta$ coupling $C_5^A(0) = 1.00 \pm 0.11$ according to the determination of Ref. [36]. The curves labeled as Δ, N, and π stand for the partial contributions of the $(\Delta P + C\Delta P)$, $(NP + CNP)$, and πEx mechanisms, respectively. The D_{13}, P_{11}, and S_{11} curves show the contribution of the different $(RP + CRP)$ terms driven by the N^* resonances. Finally, the lines labeled "no N^*" display the predicted cross section without the N^* contributions.

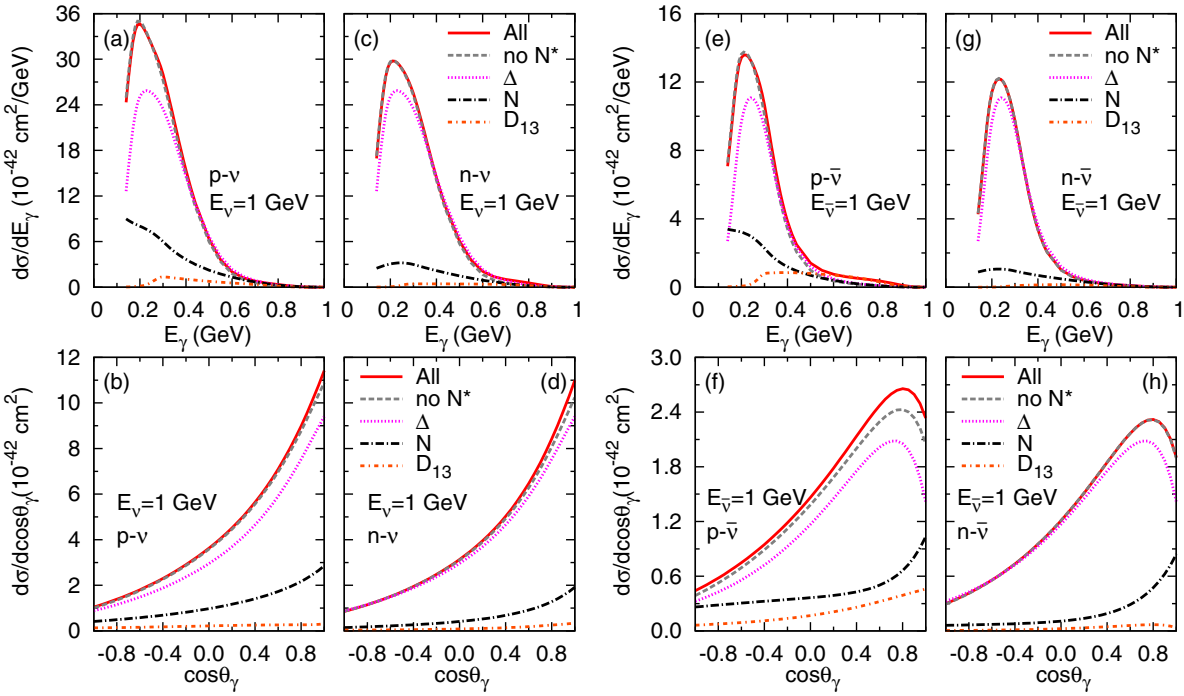

FIG. 6. (Color online) $\nu N \to \nu N\gamma$ (left) and $\bar{\nu}N \to \bar{\nu}N\gamma$ (right) photon energy (top) and photon angular (bottom) differential cross sections at $E_{\nu,\bar{\nu}} = 1$ GeV on both protons and neutrons. The angle θ_γ is referred to the direction of the incoming (anti)neutrino beam. A cut of $E_\gamma \geqslant 140$ MeV was applied. Solid curves are for the full model. The curves labeled as Δ, N, and D_{13} stand for the partial contributions of the $(\Delta P + C\Delta P)$, $(NP + CNP)$, and the $[N(1520)P + CN(1520)P]$ terms, respectively. The lines labeled "no N^*" display the predictions neglecting the N^* contributions.

At the lower energy the reaction is more forward peaked for neutrinos than for antineutrinos. In the later case, the maximum of the distribution moves forward as the energy increases. The photon energy differential cross sections always exhibit a peak slightly above $E_\gamma = 0.2$ GeV, mainly produced by the interplay between the $\Delta-$ pole and the three-body phase space photon energy distribution. The Δ propagator suppresses not only the low photon energy contributions, but also the high

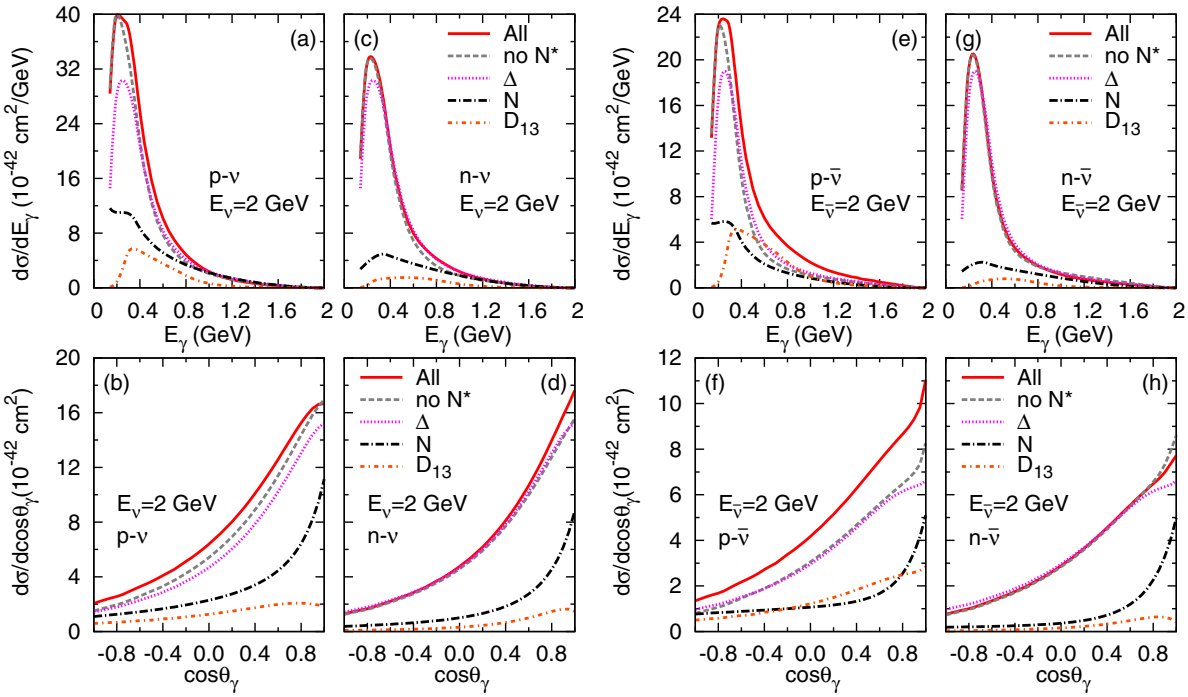

FIG. 7. (Color online) Same as Fig. 6, but for an (anti)neutrino energy of 2 GeV.

photon energy tail that would appear because of the boost to the LAB frame.

Next, we compare our predictions for the nucleon cross sections with those obtained in Refs. [58,60]. These two models include the $NP + CNP$ and $\Delta P + C\Delta P$ mechanisms, with dominance of ΔP like in our case. The Compton-like contributions ($NP + CNP$) are determined by the electromagnetic and axial nucleon form factors, which are reasonably well constrained. The predictions of Ref. [60] for these mechanisms are similar to ours. Instead, those in Ref. [58] exhibit a steeper energy dependence, because of the higher nucleon axial mass, $M_A = 1.2$ GeV in F_A [Eq. (20)], used there. This choice was motivated by the first phenomenological analysis of the MiniBooNE CCQE scattering data on carbon using the relativistic Fermi gas model [105].[9] Later theoretical studies [22,30,106,107] have shown that such high values of M_A encoded multinucleon contributions that were not taken into account in the experimental analyses. We use a lower value for $M_A = 1$ GeV, which is consistent with two independent experimental sources: bubble chamber neutrino- or antineutrino-induced QE reactions on hydrogen and deuterium, and pion electroproduction [77]. In addition to the $NP + CNP$ and $\Delta P + C\Delta P$ mechanisms, Hill [58] also considers t-channel π, ρ, and ω exchanges. Only the latter one provides a non-negligible cross section that, for antineutrinos, could become comparable to the nucleon Compton-like contribution for incident energies above 1.5 GeV. However, the size of the ω contribution strongly depends on the mostly undetermined off-shell form factor and is then affected by large uncertainties.

In the model of Zhang and Serot [60], additional contact terms allowed by symmetry were considered. As pointed out in the Introduction, they notably increase the cross section above $\sim$1 GeV (see Fig. 3 of that reference). In Ref. [38], it is argued that these contact terms are the low-energy manifestation of anomalous ρ and ω interactions; their contributions below 550 MeV are very small, as expected on the base of the power counting established there. To extend these findings to higher energies, phenomenological form factors are employed [60], which are, however, not well understood. Therefore, their cross section above $E_\nu \sim 1$ GeV should be taken cautiously once contact terms are a source of uncontrolled systematics.

We now focus on the comparison for the dominant Δ contribution, which is presented in Fig. 8. Different values of the axial $N\Delta$ coupling $C_5^A(0)$ and photon energy cuts have been implemented in Refs. [58,60], as specified in the caption of Fig. 8. We have used these inputs and compared our predictions with those found in these references, finding a good agreement particularly with Ref. [60]. In the case of Ref. [58] the agreement is better for antineutrinos than for neutrinos. However, in the actual calculations, a major difference arises from the fact that we are using a substantially lower value of $C_5^A(0) = 1.00$. Thus, our final predictions for the dominant Δ contribution are about 30% or 45% smaller than those of Refs. [60] and [58], respectively. The error bands in our results

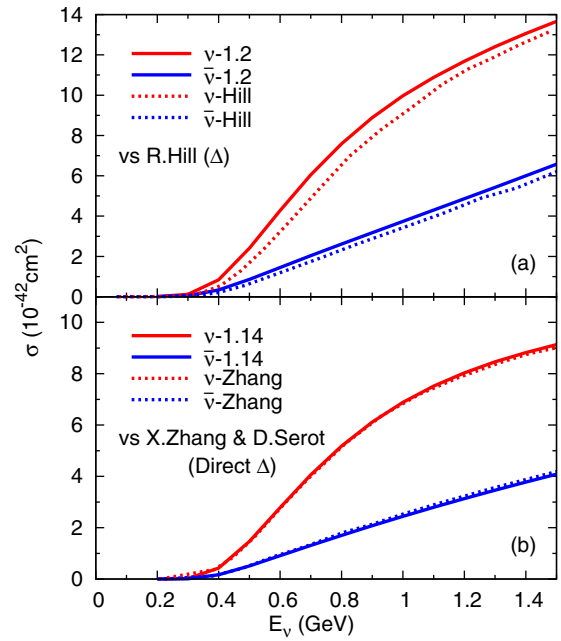

FIG. 8. (Color online) (Top panel) $\Delta P + C\Delta P$ cross sections obtained by us (solid lines) and from Ref. [58] (dashed lines), for $\nu N \to \nu N\gamma$ (red upper curves) and for $\bar{\nu}N \to \bar{\nu}N\gamma$ (blue lower curves). For this comparison we have taken $C_5^A(0) = 1.2$ and no cut in E_γ as in Ref. [58]. (Bottom panel) ΔP cross section obtained by us (solid lines) and from Ref. [60] (dashed lines), for $\nu N \to \nu N\gamma$ (red upper curves) and for $\bar{\nu}N \to \bar{\nu}N\gamma$ (blue lower curves). For this comparison we have adopted $C_5^A(0) = 1.14$ and an $E_\gamma \geqslant 0.2$ GeV cut, as in Ref. [60].

of Fig. 5, which are determined by the uncertainty in $C_5^A(0)$, partially englobe these discrepancies. In this context, it is worth remembering that the value of $C_5^A(0) = 1.00 \pm 0.11$ used here was determined in a combined analysis of the neutrino-induced pion production ANL [108,109] and BNL [110,111] bubble chamber data. This was done with a model closely resembling the present one, i.e., including nonresonant mechanisms, with the correct threshold behavior dictated by chiral symmetry, the dominant $\Delta(1232)$ excitation and also deuteron effects [36]. Such a consistency with pion production data on the nucleon was not attempted in Refs. [58,60]. Actually, the ANL $\nu_\mu p \to \mu^- p\pi^+$ data are notably overestimated in Ref. [60] as can be seen in Fig. 2 of that article.

B. Neutral-current photon emission in nuclei

For the present computations we take nuclear charge density distributions, normalized to the number of protons in the nucleus, extracted from electron scattering data [112]. The neutron matter density profiles are parametrized in the same way as the charge densities (but normalized to the number of neutrons) with small changes from Hartree-Fock calculations [113] and supported by pionic atom data [114]. The corresponding parameters are compiled in Table I of Ref. [92]. Furthermore, these density distributions have been deconvoluted to get center-point densities following the procedure described in Ref. [115].

[9] In the final MiniBooNE analysis [2], an even larger value of $M_A \sim 1.35$ GeV was obtained.

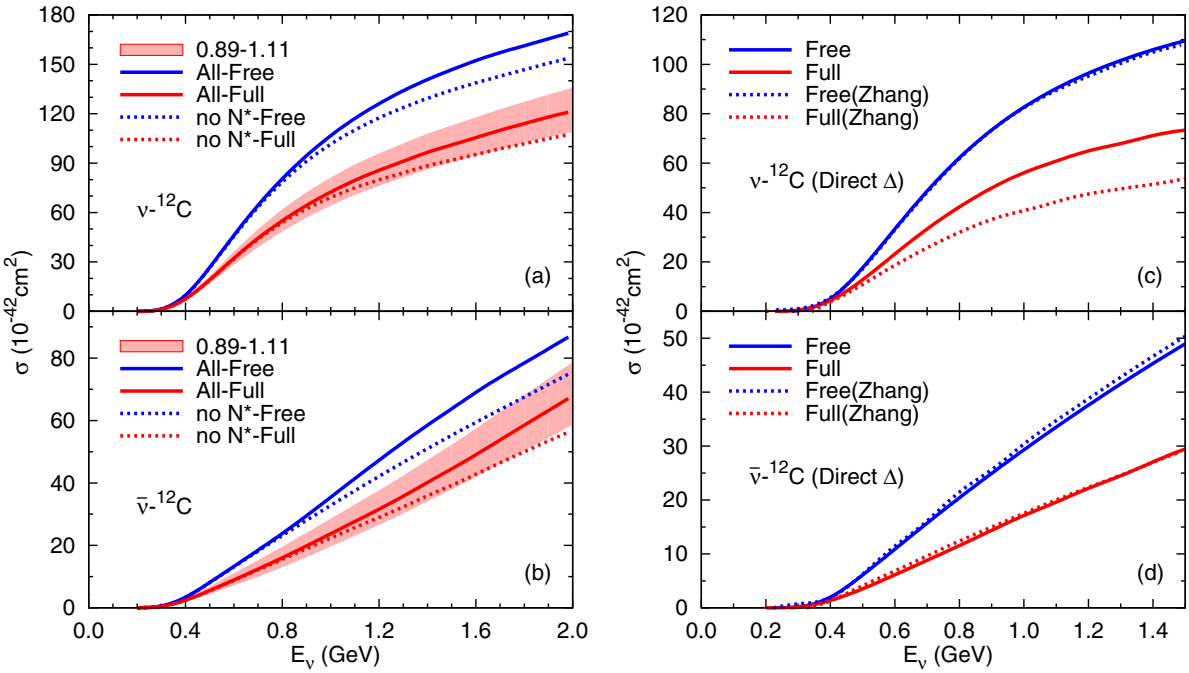

FIG. 9. (Color online) (Left panel) Neutrino (top) and antineutrino (bottom) incoherent photon emission cross sections on ^{12}C. All curves in this panel have been obtained with an $E_\gamma \geqslant 140$ MeV cut in the phase space. Solid lines stand for results from the complete model at the nucleon level, while the dotted lines display the predicted cross sections without the N^* contributions. Curves denoted as "Free" (upper blue curves) do not include any nuclear correction; the nuclear target is treated as a mere ensemble of nucleons ($\sigma_A = Z\sigma_p + N\sigma_n$). Curves labeled as "Full" (lower red curves) take into account Pauli blocking, Fermi motion, and the in-medium Δ resonance broadening. The error bands show the uncertainty on the full model that arises from the determination of the axial $N\Delta$ coupling from data ($C_5^A(0) = 1.00 \pm 0.11$) [36]. (Right panel) ΔP contribution to the neutrino (top) and antineutrino (bottom) photon emission cross sections on ^{12}C from Ref. [60] compared to our predictions for the same mechanism, adopting the same infrared photon energy cut $E_\gamma \geqslant 0.2$ GeV and $C_5^A(0) = 1.14$. The meaning of "Free" and "Full" labels is the same as in the left plots.

1. *Incoherent reaction:* $\mathbf{1p1h\gamma}$ *contribution*

In the left panels of Fig. 9, we show our predictions for the (anti)neutrino incoherent photon emission cross sections on ^{12}C as a function of the (anti)neutrino energy up to 2 GeV. We observe that the neglect of nuclear medium corrections, as it was done in the study of the NCγ excess of events at MiniBooNE of Ref. [62], is a quite poor approximation. By taking into account Fermi motion and Pauli blocking, the cross section already goes down by more than 10%. With the full model that also includes the Δ resonance in-medium modification, the reduction is of the order of 30%. Furthermore, we corroborate the findings on nucleon targets (Fig. 5) about the N^* contributions [mostly the $N(1520)$] being sizable above $\sim$1.5 GeV, specially for antineutrino cross sections.

In the right-hand plots of Fig. 9, we compare our results with the predictions of Ref. [60]. As in the nucleon case (Fig. 8), we focus on the dominant ΔP contribution and use the same $C_5^A(0) = 1.14$ value and photon energy cut (200 MeV) as in Ref. [60]. When all the nuclear corrections are neglected, we certainly obtain the same curves as in Fig. 8, but multiplied by the number of nucleons (12). As can be observed in the figure, we find an excellent agreement both for neutrino and antineutrino cross sections. However, nuclear medium effects turn out to be much more important, leading to a much larger suppression ($\sim$50%), in the calculation of Ref. [60] for neutrinos. This seems surprising, first, because at these moderately high neutrino energies, similar nuclear corrections should be obtained with both models. In particular, one would not expect significant differences in the Δ resonance broadening in the medium when calculated with Eq. (66) or with the spreading potential of Ref. [48].[10] Because of the larger nuclear suppression, the ΔP cross section found in Ref. [60] is smaller than the one obtained here in spite of the 14% larger $C_5^A(0)$. In the antineutrino cross sections, the difference is not so large, and the medium effects shown in Ref. [60] are only slightly greater than those found in the present work. As a consequence of the large reduction of the ΔP contribution on ^{12}C, the contact terms become relatively important from $E_\nu = 1$ GeV on, rapidly increasing and turning dominant above 1.5 GeV (see Fig. 3 of Ref. [60]). Indeed, contact terms compensate the suppression of the ΔP mechanism, so that the incoherent cross sections predicted in Ref. [60] are comparable to ours in the 1-GeV region, but become about 40% (70%) larger than our results for 2-GeV neutrinos (antineutrinos) even though the contributions from resonances heavier that the Δ were not taken into account.

[10] We should mention that we agree better with the ΔP cross section of Ref. [60] for neutrinos if we take an imaginary part of the Δ self-energy twice bigger than the one in Eq. (66).

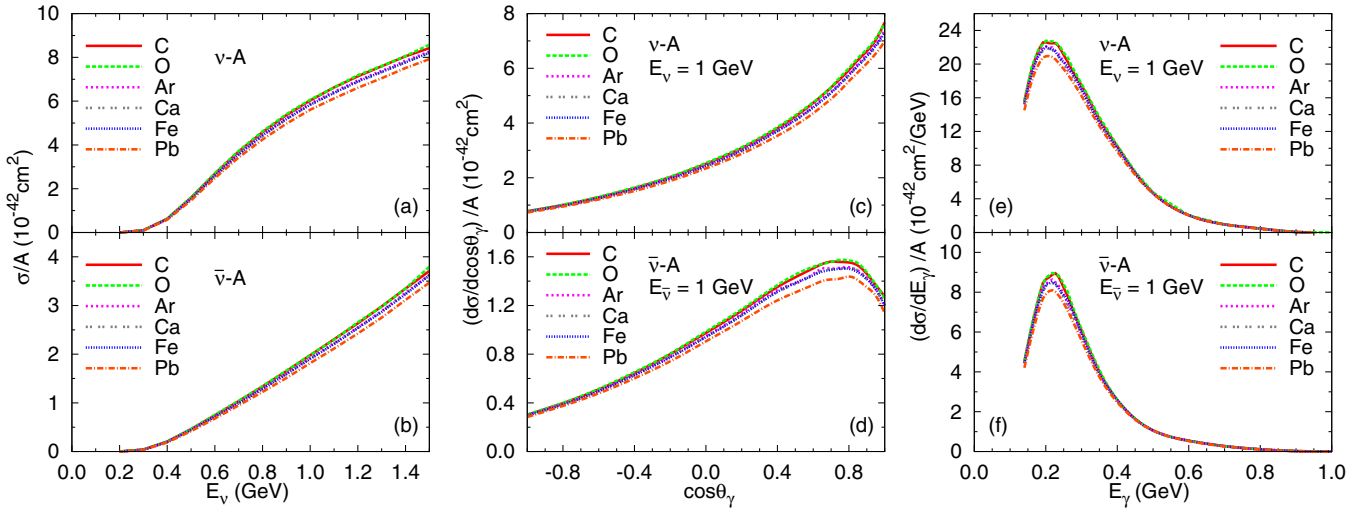

FIG. 10. (Color online) Neutrino (top) and antineutrino (bottom) incoherent NCγ total cross sections as a function of the (anti)neutrino energy (left panels), photon angular (middle panels), and photon energy (right panels) differential distributions at $E_{\nu,\bar{\nu}}$ =1 GeV. The angle θ_γ is referred to the direction of the incoming (anti)neutrino beam. Results for different nuclei (^{12}C,^{16}O,^{40}Ar, ^{40}Ca,^{56}Fe, and ^{208}Pb) divided by the number of nucleons are shown. All results are obtained with the full model, including nuclear effects and implementing an $E_\gamma \geqslant 140$ MeV cut.

In Fig. 10, we show total NCγ incoherent cross sections for different nuclei (carbon, oxygen, argon, calcium, iron, and lead) as a function of the (anti)neutrino energy. We also display photon angular and energy distributions for an incoming (anti)neutrino energy of 1 GeV. We notice the approximated A scaling present in the results, which implies a mild A dependence of nuclear effects. Nevertheless, the cross section is smaller for heavier nuclei, particularly ^{208}Pb. We should stress that the observed deviation from scaling cannot be explained only by neutron cross sections being smaller than proton ones (around 15%–20% at $E_\nu \sim 1.5$ GeV).[11]

Concerning the kinematics of the emitted photons, the main features are similar to those in Figs. 6 and 7 for scattering on single nucleons. As in that case, the reaction is more forward for neutrinos than for antineutrinos at $E_\nu = 1$ GeV. In the outgoing photon energy distributions (right panels), the peak just above $E_\gamma = 0.2$ GeV observed for nucleons is reproduced here without any shift in the peak position but with slightly larger width as the target mass increases.

2. *Coherent reaction*

Total NCγ coherent cross sections on carbon as a function of the (anti)neutrino energy are presented in Fig. 11. We display our results from the full calculation, from $(\Delta P + C\Delta P)$ alone, and without the mechanisms from the second N^* resonance region. The N^* contributions are quite small in the coherent channel, while the Δ is absolutely dominant in both the neutrino and the antineutrino modes. Nucleon-pole contributions are negligible because the coherent kinematics favors a strong cancellation between the direct and crossed terms of the amplitude. A similar effect was observed in weak coherent pion production [68].

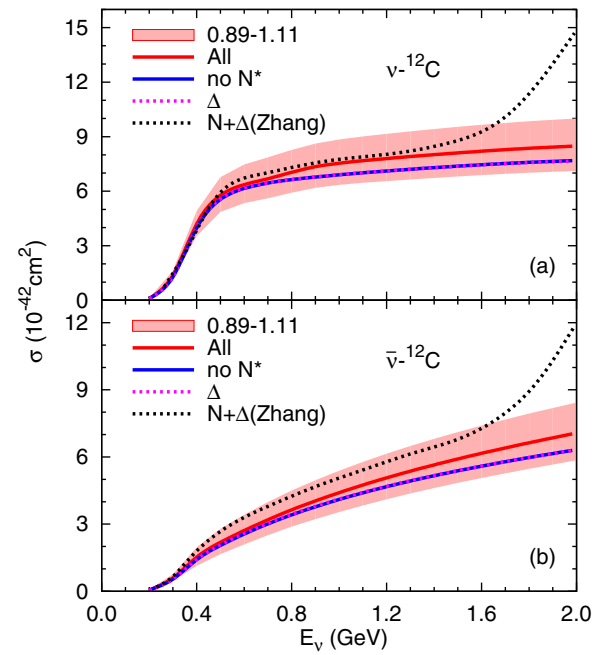

FIG. 11. (Color online) Neutrino (top) and antineutrino (bottom) total NCγ coherent cross sections on ^{12}C, as a function of the (anti)neutrino energy. A photon energy cut of $E_\gamma \geqslant 140$ MeV was implemented. Red solid lines stand for results from the complete model derived in this work, including Δ resonance broadening, with error bands determined by the uncertainty of ± 0.11 in $C_5^A(0)$ [36]. The solid blue lines below, labeled as "no N^*", display the predicted cross sections without the N^* amplitudes, while the magenta dotted ones are the contributions from the $(\Delta P + C\Delta P)$ mechanisms. We also show the predictions of Ref. [60] for nucleon and Δ mechanisms (red solid lines in Fig. 4 of this reference).

[11]Note that the ΔP contribution is the same on protons and neutrons. Thus, this dominant mechanism does not contribute to such differences.

For comparison, the predictions from the ($\Delta P + C\Delta P + NP + CNP$) part of the model of Ref. [60] are also plotted. They are slightly above our corresponding results (without N^*), and within the uncertainty band of our full-model curve, up to (anti)neutrino energies of 1.4–1.5 GeV. Above these energies, there is a a change of slope and a pronounced enhancement [60]. Moreover, in the model of this reference, the cross section above $E_{\nu,\bar{\nu}} = 0.65$ GeV is not dominated by the $(N + \Delta)$ mechanism, but by contact terms from higher order effective Lagrangians whose extrapolation to higher energies is uncertain. Indeed, for some choices of parameters, coherent cross sections as large as 25×10^{-42} cm^2 were obtained for $E_{\nu,\bar{\nu}} = 1.5$ GeV [60]. This amounts to a factor 3–4 larger than our predictions. We should remind here that below 500 MeV, the contact terms in the nucleon amplitudes are very small as expected based on the power counting established in Ref. [38]. Because of the substantial reduction of the Δ mechanisms, the contact terms in Ref. [60] acquire further relevance when the processes take place in nuclei, especially for the coherent reaction.

Our results for coherent NCγ total and differential cross sections on different nuclei are shown in Fig. 12. Neutrino (antineutrino) coherent cross sections are about a factor 15 (10) smaller than the incoherent ones given in Fig. 10. Thus, the relative relevance of the coherent channel with respect to the incoherent channel is comparable, if not greater than in the pion production reactions induced by neutrinos and antineutrinos, where it is of the order of a few percent [39,95]. Notice that in these latter reactions the coherent cross section is further reduced (by around a factor of two) because of the strong distortion of the outgoing pion, which is not present in photon production. It is also true that the incoherent cross section is reduced (∼20%–30%) by final state interactions, again absent for photons.

The coherent cross sections neither scale with A, like the incoherent one approximately does, nor with A^2 as one would expect from the coherence of the dominant isoscalar ΔP mechanism (sum of neutron and proton amplitudes). This is due to the presence of the nuclear form factor (Fourier transform of the nuclear density for momentum $\vec{q} - \vec{k}_\gamma$); see the first paragraph of Sec. III B and Eq. (70). The nuclear form factor gets its maximum values when $\vec{q} = \vec{k}_\gamma$, which corresponds to $q^2 = 0$. In this forward kinematics, the lepton tensor $L^{(\nu,\bar{\nu})}_{\mu\sigma} \sim q_\mu q_\sigma$, and the vector part of the amplitude squared is zero due to CVC. Furthermore, the axial contribution, which is purely transverse $\sim(\vec{k}_\gamma \times \vec{q})$ also vanishes. Therefore, the largest differential cross sections arise in kinematics that optimize the product of the amplitude squared of the elementary process times the nuclear form factor. Such a balance also appears in the (^{3}He,^{3}H π^+) reaction on nuclear targets [96] or in electron- and photon-induced reactions, making the electromagnetic coherent pion production cross section a rather small fraction of the total inclusive nuclear absorption one [74,75].

The described pattern strongly influences the photon angular dependence of this reaction shown in the middle panels of Fig. 12 although in a nontrivial way because the θ_γ angle is given with respect to the direction of the incoming (anti)neutrino beam; it is not the angle formed by $\vec{q}$ and $\vec{k}_\gamma$, which is not observable. Actually, for each value of θ_γ, and integration over all possible $\vec{q}$ is carried out. The details of the angular distributions are determined by interferences between the dominant ΔP mechanism and the $C\Delta P$ and $N(1520)$ ones, enhanced by the kinematic constrains imposed by the nuclear form factor. The impact of the latter is apparent in the width of the angular distributions which are narrower for heavier nuclei.

Finally, in Fig. 12 we display the outgoing photon energy distributions (right panels). In the coherent NCγ reaction, there are two massless particles in the final state, and a third one (the nucleus) which is very massive and has a small (negligible) kinetic energy but can carry large momenta. The prominent peak observed for all nuclei is due to the dominant

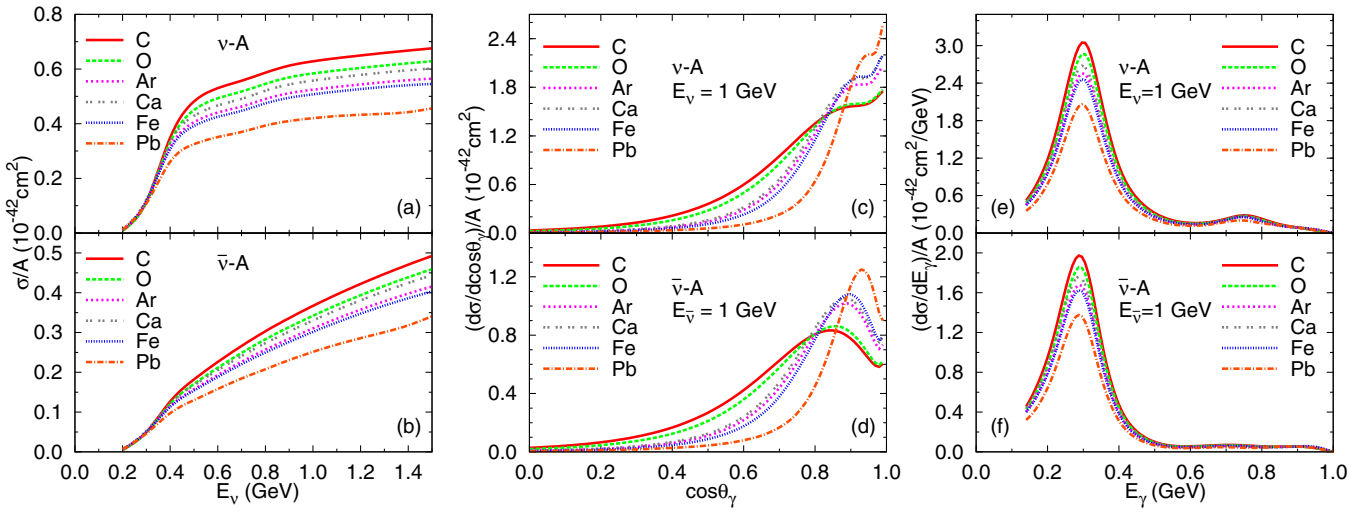

FIG. 12. (Color online) Neutrino (top) and antineutrino (bottom) total cross sections (left panels) photon angular (middle panels) and photon energy (right panels) differential distributions for the coherent NCγ reaction, obtained with our full model. The angle θ_γ is referred to the direction of the incoming (anti)neutrino beam. The kinematic region of $E_\gamma < 140$ MeV was cut out. Results for different nuclei (^{12}C,^{16}O,^{40}Ar, ^{40}Ca,^{56}Fe, and ^{208}Pb) divided by the number of nucleons are shown.

Δ resonance[12] shifted to slightly lower invariant masses mostly by the energy dependence of the Δ width and the interference with the $C\Delta P$ mechanism. The peak position does not change appreciably from nucleus to nucleus, but it gets broader as A increases. The second, smaller, and broader peak that can be discerned for neutrinos but not for antineutrinos corresponds to the excitation of the $D_{13}(1520)$ resonance.

V. CONCLUSIONS

Neutral-current photon emission on nucleons and nuclei at intermediate energies has been theoretically investigated. We have developed a microscopic model for these reactions, in line with previous work on weak pion production [35,39,46,68]. We have critically reviewed previous models for the NCγ reaction on single nucleons [38,58,60] and nuclei [48,60,63] and compared our results with those found in these references. From such a comparison, we have identified some aspects of the above studies that either needed to be improved or that were sources of uncontrolled systematic corrections.

NCγ processes are important backgrounds for $\nu_\mu \to \nu_e$ and $\bar{\nu}_\mu \to \bar{\nu}_e$ appearance oscillation experiments when photons are misidentified as $e^\pm$ from CCQE scattering of $\nu_e(\bar{\nu}_e)$. At the relevant energies for MiniBooNE and T2K experiments, the reaction is dominated by the weak excitation of the $\Delta(1232)$ resonance and its subsequent decay into $N\gamma$. In addition, we have also considered nonresonant amplitudes that, close to threshold, are fully determined by chiral symmetry, and those driven by nucleon excited states from the second resonance region. Among the latter ones, we have found a sizable contribution of the $D_{13}(1520)$ state for (anti)neutrino energies above 1.5 GeV.

The model on the nucleon is extended to nuclear targets taking into account Fermi motion, Pauli blocking, and the in-medium modifications of the Δ properties in a local Fermi gas, with Fermi momenta determined from proton and neutron density distributions. We have predicted different observables for several nuclei, including some of the common ones in current and future neutrino detectors (carbon, oxygen, argon, iron). The importance of nuclear corrections in both the coherent and incoherent channels has been stressed. The A dependence of the cross section, which is different for the coherent and incoherent reactions, has been also discussed.

In light of our results, a new analysis of the NC-induced photon production at MiniBooNE with the present model, aiming at the clarification of the role played by NCγ events in the low-energy excess observed in this experiment, looks timely and important. It will be the subject of future research.

ACKNOWLEDGMENTS

We thank M. J. Vicente Vacas for helpful discussions and M. Valverde for collaboration in an early stage of this project. This research was supported by the Spanish Ministerio de Economía y Competitividad and European FEDER funds under Contracts No. FIS2011-28853-C02-01 and No. FIS2011-28853-C02-02 and the Spanish Consolider-Ingenio 2010 Program CPAN (Contract No. CSD2007-00042), the Generalitat Valenciana under Contract No. PROMETEO/2009/0090, and the EU HadronPhysics3 project (Grant No. 283286).

APPENDIX A: RELATIONS BETWEEN ELECTROMAGNETIC FORM FACTORS AND HELICITY AMPLITUDES

The $\gamma N \to R$ helicity amplitudes describe the nucleon-resonance transition depending on the polarization of the incoming virtual photon and the baryon-spin projections onto the direction of the photon momentum. We follow the definitions adopted in the MAID analysis [82,83], from which the empirical parametrizations of the helicity amplitudes are taken. Namely[13]

$$\mathcal{A}_{1/2} = \sqrt{\frac{2\pi\alpha}{k_R}} \left\langle S_z^* = \frac{1}{2} \middle| \epsilon_\mu^{(+)} J^\mu_{\rm EM} \middle| S_z = -\frac{1}{2} \right\rangle \frac{1}{\sqrt{2M}\sqrt{2M_R}}, \tag{A1}$$

$$\mathcal{A}_{3/2} = \sqrt{\frac{2\pi\alpha}{k_R}} \left\langle S_z^* = \frac{3}{2} \middle| \epsilon_\mu^{(+)} J^\mu_{\rm EM} \middle| S_z = \frac{1}{2} \right\rangle \frac{1}{\sqrt{2M}\sqrt{2M_R}}, \tag{A2}$$

$$\mathcal{S}_{1/2} = -\sqrt{\frac{2\pi\alpha}{k_R}} \left\langle S_z^* = \frac{1}{2} \middle| \frac{|\vec{k}\,|}{\sqrt{Q^2}} \epsilon_\mu^{(0)} J^\mu_{\rm EM} \middle| S_z = \frac{1}{2} \right\rangle \times \frac{1}{\sqrt{2M}\sqrt{2M_R}}, \tag{A3}$$

in the resonance rest frame (notice that $S_{1/2}$ is not Lorentz invariant) and with the z axis parallel to the photon momentum. In other words,

$$\begin{aligned} k^\mu &= (k^0,0,0,|\vec{k}|), \\ p^\mu &= (\sqrt{M^2+\vec{k}^2},0,0,-|\vec{k}|), \\ p^{*\mu} &= (p+k)^\mu = (M_R,0,0,0) \end{aligned} \tag{A4}$$

are the virtual photon, nucleon, and resonance four-momenta. In addition, $Q^2 = -k^2$ and

$$k_R = \frac{M_R^2 - M^2}{2M_R}. \tag{A5}$$

The photon polarization vectors are given by

$$\epsilon^\mu_{(\pm)} = \mp\frac{1}{\sqrt{2}}(0,1,\pm i,0), \quad \epsilon^\mu_{(0)} = \frac{1}{\sqrt{Q^2}}(|\vec{k}\,|,0,0,k^0). \tag{A6}$$

Finally, S_z (S_z^*) denotes the nucleon (resonance) spin projection onto the z axis.

[12] The energy of the resonant photons in LAB can be estimated from $M_R^2 \approx (k_\gamma + p')^2$. Taking p' from Equation (73) and for the situation $\vec{k}_\gamma \approx \vec{q}$ favored by the nuclear form factor, one finds that $k^0_{\gamma(R)} \approx (M_R^2 - M^2)/(2M)$. This gives 340 MeV for the $\Delta(1232)$ and 760 MeV for the $N(1520)$.

[13] It should be pointed out that the $1/(\sqrt{2M}\sqrt{2M_R})$ factor in the definition of the helicity amplitudes comes from the normalization of Dirac spinors ($\bar{u}u = 2M, \bar{u}_R u_R = 2M_R$) adopted in the present work.

With these definitions and the currents of Sec. II B, it is straightforward to derive the following equations connecting helicity amplitudes and electromagnetic form factors [37].

a. $N(1440)$

$$A_{1/2}^{p,n} = \sqrt{\frac{\pi\alpha[(M_R - M)^2 + Q^2]}{2M(M_R^2 - M^2)}}\left[\frac{Q^2}{2M^2}F_1^{p,n} + \frac{M_R + M}{M}F_2^{p,n}\right], \tag{A7}$$

$$S_{1/2}^{p,n} = -\sqrt{\frac{\pi\alpha[(M_R + M)^2 + Q^2]}{M(M_R^2 - M^2)}}\frac{(M_R - M)^2 + Q^2}{4MM_R}\left[\frac{M_R + M}{2M}F_1^{p,n} - F_2^{p,n}\right]. \tag{A8}$$

b. $N(1535)$

$$A_{1/2}^{p,n} = \sqrt{\frac{\pi\alpha[(M_R + M)^2 + Q^2]}{2M(M_R^2 - M^2)}}\left[\frac{Q^2}{2M^2}F_1^{p,n} + \frac{M_R - M}{M}F_2^{p,n}\right], \tag{A9}$$

$$S_{1/2}^{p,n} = \sqrt{\frac{\pi\alpha[(M_R - M)^2 + Q^2]}{M(M_R^2 - M^2)}}\frac{(M_R + M)^2 + Q^2}{4MM_R}\left[\frac{M_R - M}{2M}F_1^{p,n} - F_2^{p,n}\right]. \tag{A10}$$

c. $\Delta(1232)$

$$A_{1/2}^{p,n} = \sqrt{\frac{\pi\alpha[(M_R - M)^2 + Q^2]}{3M(M_R^2 - M^2)}}\left[\frac{M^2 + MM_R + Q^2}{MM_R}C_3^V - \frac{M_R^2 - M^2 - Q^2}{2M^2}C_4^V - \frac{M_R^2 - M^2 + Q^2}{2M^2}C_5^V\right]. \tag{A11}$$

$$A_{3/2}^{p,n} = \sqrt{\frac{\pi\alpha[(M_R - M)^2 + Q^2]}{M(M_R^2 - M^2)}}\left[\frac{M + M_R}{M}C_3^V + \frac{M_R^2 - M^2 - Q^2}{2M^2}C_4^V + \frac{M_R^2 - M^2 + Q^2}{2M^2}C_5^V\right]. \tag{A12}$$

$$S_{1/2}^{p,n} = \sqrt{\frac{\pi\alpha[(M_R + M)^2 + Q^2]}{6M(M_R^2 - M^2)}}\frac{(M_R - M)^2 + Q^2}{M_R^2}\left[\frac{M_R}{M}C_3^V + \frac{M_R^2}{M^2}C_4^V + \frac{M_R^2 + M^2 + Q^2}{2M^2}C_5^V\right]. \tag{A13}$$

d. $N(1520)$

$$A_{1/2}^{p,n} = \sqrt{\frac{\pi\alpha[(M_R + M)^2 + Q^2]}{3M(M_R^2 - M^2)}}\left[\frac{M^2 - MM_R + Q^2}{MM_R}C_3^{p,n} - \frac{M_R^2 - M^2 - Q^2}{2M^2}C_4^{p,n} - \frac{M_R^2 - M^2 + Q^2}{2M^2}C_5^{p,n}\right], \tag{A14}$$

$$A_{3/2}^{p,n} = \sqrt{\frac{\pi\alpha[(M_R + M)^2 + Q^2]}{M(M_R^2 - M^2)}}\left[\frac{M - M_R}{M}C_3^{p,n} - \frac{M_R^2 - M^2 - Q^2}{2M^2}C_4^{p,n} - \frac{M_R^2 - M^2 + Q^2}{2M^2}C_5^{p,n}\right] \tag{A15}$$

$$S_{1/2}^{p,n} = -\sqrt{\frac{\pi\alpha[(M_R - M)^2 + Q^2]}{6M(M_R^2 - M^2)}}\frac{(M_R + M)^2 + Q^2}{M_R^2}\left[\frac{M_R}{M}C_3^{p,n} + \frac{M_R^2}{M^2}C_4^{p,n} + \frac{M_R^2 + M^2 + Q^2}{2M^2}C_5^{p,n}\right]. \tag{A16}$$

APPENDIX B: OFF-DIAGONAL GOLDBERGER-TREIMAN RELATIONS

We consider an effective Lagrangian for the $RN\pi$ vertex, which is then used to calculate the πN decay width of the resonance. Using the Particle Data Group (PDG) [86] values for the decay width and πN branching ratio, one can fix the $RN\pi$ coupling. Thanks to PCAC,

$$\partial_\mu A_{\rm NCI}^\mu(x) = 2 f_\pi m_\pi^2 \pi^0, \tag{B1}$$

the latter coupling can be related to the dominant axial coupling in $A_{\rm NCI}^\mu$, which is the isovector part of the neutral current. This is the so-called off-diagonal GT relation. It establishes that in the soft pion limit,

$$p_{\pi^0}^\mu \langle R|A_\mu^{\rm NCI}(0)|N\rangle = -2if_\pi \langle R|\mathcal{L}_{{\rm RN}\pi}|N\pi^0\rangle. \tag{B2}$$

As in Refs. [37,65], we distinguish between different cases, depending on the spin, parity, and isospin of the resonance. Let us start with spin $1/2$ states with isospin $1/2$, like the $P_{11}(1440)$ and $S_{11}(1535)$. In this case,

$$\mathcal{L}_{R_{1/2}N\pi} = \frac{f}{m_\pi}\bar\Psi \begin{Bmatrix}\gamma^\mu\gamma_5\\ \gamma^\mu\end{Bmatrix}(\partial_\mu\vec\pi\cdot\vec\tau)\Psi_{R_{1/2}} + {\rm H.c.}, \tag{B3}$$

where Ψ, $\Psi_{R_{1/2}}$, and $\vec\pi$ are the nucleon, resonance, and pion fields;[14] $\vec\tau$ are the isospin Pauli matrices. The upper (lower) Lagrangian holds for positive (negative) parity resonances. The partial $R \to \pi N$ decay width is

$$\Gamma_{R_{1/2}\to N\pi} = \frac{3}{4\pi M_R}\left(\frac{f}{m_\pi}\right)^2 (M_R \pm M)^2 (E_N \mp M)|\vec p_N|, \tag{B4}$$

[14]Our convention is such that $(\pi^1 - i\pi^2)/\sqrt{2}$ creates a π^- or annihilates a π^+ while a $\pi^3 = \pi^0$ field creates or annihilates a π^0.

where

$$E_N = \sqrt{M^2 + \vec{p}_N^{\,2}} = \frac{M_R^2 + M^2 - m_\pi^2}{2M_R}. \tag{B5}$$

The upper (lower) signs in Eq. (B4) stand for positive (negative) parity resonances. The off-diagonal GT relation amounts to

$$F_{A(R)}(0) = -2\frac{f}{m_\pi} f_\pi, \tag{B6}$$

regardless of the parity. The coupling $F_{A(R)}(0)$ defined in Eq. (36) is now expressed in terms of f/m_π extracted from the $R \to \pi N$ decay width given above.

For $J = 3/2$ resonances, $\Delta(1232)$ and $D_{13}(1520)$ in our case,

$$\mathcal{L}_{R_{3/2}N\pi} = \frac{f^*}{m_\pi}\bar{\Psi}\begin{Bmatrix} 1 \\ \gamma_5 \end{Bmatrix}(\partial_\mu\vec{\phi}\cdot\vec{\mathbf{t}})\Psi^\mu_{R_{3/2}} + \text{H.c.}, \tag{B7}$$

where $\Psi^\mu_{R_{3/2}}$ is the resonance spin 3/2 field in the Rarita-Schwinger representation; $\vec{\mathbf{t}} = \vec{\tau}$ stands for isospin 1/2 resonances and $\vec{\mathbf{t}} = \vec{\mathbf{T}}$ (3/2 to 1/2 isospin transition operator)[15] for isospin 3/2 ones. The upper (lower) Lagrangian applies for positive (negative) parity states. The partial $R \to \pi N$ decay width is then given by

$$\Gamma_{R_{3/2}\to N\pi} = \frac{c_I}{6\pi}\left(\frac{f^*}{m_\pi}\right)^2 \frac{E_N \pm M}{2M_R}|\vec{p}_N|^3, \tag{B8}$$

where the upper (lower) sign stands for positive (negative) parity resonances while $c_I = 1(3)$ for isospin 1/2 (3/2). Then we deduce

$$C^A_{5(R)}(0) = d_I\frac{f^*}{m_\pi} f_\pi, \tag{B9}$$

where the numerical value of f^*/m_π is obtained from Eq. (B8). The coefficient $d_I = -2$ is for isospin 1/2 states like the $D_{13}(1520)$ and $d_I = \sqrt{2/3}$ for isospin 3/2 ones, like the $\Delta(1232)$. The corresponding $C^A_{5(R)}(0)$ couplings determined by this GT relation were defined in Eqs. (42) and (29). It should be reminded that for the $N - \Delta(1232)$ transition, rather than the $C^A_5(0)$ value from Eq. (B9), we use the one fitted in Ref. [36] to the $\nu_\mu p \to \mu^- p\pi^+$ ANL and BNL bubble chamber data.

APPENDIX C: DECAY MODES OF THE SECOND REGION RESONANCES

In Table II, we compile the most relevant $P_{11}(1440)$, $D_{13}(1520)$, and $S_{11}(1535)$ decay modes and their branching ratios, taking values within the ranges of the PDG estimates [86].

TABLE II. Main decay modes, branching fractions (Γ_i/Γ), and relative angular momenta L of the decay particles, for the N^* resonances considered in this work.

$N(1440)$			$N(1520)$			$N(1535)$		
Mode	fraction(%)	L	Mode	fraction(%)	L	Mode	fraction(%)	L
$N\pi$	65	1	$N\pi$	60	2	$N\pi$	45	0
$\Delta\pi$	20	1	$\Delta\pi$	15	0	$N\eta$	42	0
$N\sigma$	15	0	$\Delta\pi$	12.5	2	$\Delta\pi$	1	2
			$N\rho$	9	0	$N\rho$	2	0
			$N\rho$	3.5	2	$N\sigma$	2	1
						$N(1440)\pi$	8	0

To obtain the partial width of a decay mode into unstable particles we use [116]

$$\Gamma_{R\to ab}(W) = \Gamma_{R\to ab}(W = M_R)\frac{\rho_{ab}(W)}{\rho_{ab}(M_R)}, \tag{C1}$$

where W denotes the resonance invariant mass. The function ρ_{ab} is given by

$$\begin{aligned}\rho_{ab}(W) &= \int d\left(p_a^2\right)d\left(p_b^2\right)\mathcal{A}\left(p_a^2\right)\mathcal{A}\left(p_b^2\right)\frac{p_{ab}^{2L+1}\left(W^2,p_a^2,p_b^2\right)}{W} \\ &\quad\times\Theta\left(W-\sqrt{p_a^2}-\sqrt{p_b^2}\right), \\ p_{ab}^2 &= \frac{\lambda\left(W^2,p_a^2,p_b^2\right)}{4W^2},\end{aligned} \tag{C2}$$

where p_{ab} denotes the center-of-mass momentum of the final state products, and L the relative angular momentum (Table II). The vacuum spectral function $\mathcal{A}_a$ reads

$$\mathcal{A}\left(p_a^2\right) = -\frac{1}{\pi}\text{Im}\left(\frac{1}{p_a^2 - M_a^2 + iM_a\Gamma_a\left(p_a^2\right)}\right). \tag{C3}$$

If one of the decay products (a) is a stable particle, then $\Gamma_a = 0$ and the vacuum spectral function can be written as

$$\mathcal{A}\left(p_a^2\right) = \delta\left(p_a^2 - M_a^2\right), \tag{C4}$$

so that ρ_{ab} becomes

$$\begin{aligned}\rho_{ab}(W) &= \frac{M_b}{\pi W}\int d\left(p_b^2\right)\frac{\Gamma_b\left(p_b^2\right)}{\left(p_b^2 - M_b^2\right)^2 + M_b^2\Gamma_b^2\left(p_b^2\right)} \\ &\quad\times p_{ab}^{2L+1}\left(W^2,M_a^2,p_b^2\right)\Theta\left(W - M_a - \sqrt{p_b^2}\right).\end{aligned} \tag{C5}$$

If both final particles are stable, then

$$\rho_{ab}(W) = \frac{p_{ab}^{2L+1}\left(W^2,M_a^2,M_b^2\right)}{W}\Theta(W - M_a - M_b). \tag{C6}$$

[15] Normalized in such a way that the isospin matrix element $\langle\frac{3}{2}\frac{3}{2}|T_1^\dagger + iT_2^\dagger|\frac{1}{2}\frac{1}{2}\rangle = -\sqrt{2}$.

[1] J. Formaggio and G. Zeller, Rev. Mod. Phys. **84**, 1307 (2012).
[2] A. A. Aguilar-Arevalo *et al.* (MiniBooNE Collaboration), Phys. Rev. D **81**, 092005 (2010).
[3] A. A. Aguilar-Arevalo *et al.* (MiniBooNE Collaboration), Phys. Rev. D **82**, 092005 (2010).
[4] A. A. Aguilar-Arevalo *et al.* (MiniBooNE Collaboration), Phys. Rev. D **88**, 032001 (2013).
[5] L. Fields *et al.* (MINERvA Collaboration), Phys. Rev. Lett. **111**, 022501 (2013).
[6] G. Fiorentini *et al.* (MINERvA Collaboration), Phys. Rev. Lett. **111**, 022502 (2013).
[7] V. Lyubushkin *et al.* (NOMAD Collaboration), Eur. Phys. J. C **63**, 355 (2009).
[8] A. A. Aguilar-Arevalo *et al.* (MiniBooNE Collaboration), Phys. Rev. D **81**, 013005 (2010).
[9] A. A. Aguilar-Arevalo *et al.* (MiniBooNE Collaboration), Phys. Rev. D **83**, 052009 (2011).
[10] A. A. Aguilar-Arevalo *et al.* (MiniBooNE Collaboration), Phys. Rev. D **83**, 052007 (2011).
[11] K. Hiraide *et al.* (SciBooNE Collaboration), Phys. Rev. D **78**, 112004 (2008).
[12] Y. Kurimoto *et al.* (SciBooNE Collaboration), Phys. Rev. D **81**, 111102 (2010).
[13] C. Kullenberg *et al.* (NOMAD Collaboration), Phys. Lett. B **682**, 177 (2009).
[14] K. Abe *et al.* (T2K Collaboration), Phys. Rev. D **87**, 092003 (2013).
[15] Y. Nakajima *et al.* (SciBooNE Collaboration), Phys. Rev. D **83**, 012005 (2011).
[16] P. Adamson *et al.* (MINOS Collaboration), Phys. Rev. D **81**, 072002 (2010).
[17] Q. Wu *et al.* (NOMAD Collaboration), Phys. Lett. B **660**, 19 (2008).
[18] J. G. Morfin, J. Nieves, and J. T. Sobczyk, Adv. High Energy Phys. **2012**, 934597 (2012).
[19] K. M. Graczyk and J. T. Sobczyk, Eur. Phys. J. C **31**, 177 (2003).
[20] J. Nieves, J. E. Amaro, and M. Valverde, Phys. Rev. C **70**, 055503 (2004).
[21] M. S. Athar, S. Ahmad, and S. Singh, Eur. Phys. J. A **24**, 459 (2005).
[22] M. Martini, M. Ericson, G. Chanfray, and J. Marteau, Phys. Rev. C **80**, 065501 (2009).
[23] O. Benhar, N. Farina, H. Nakamura, M. Sakuda, and R. Seki, Phys. Rev. D **72**, 053005 (2005).
[24] A. M. Ankowski and J. T. Sobczyk, Phys. Rev. C **77**, 044311 (2008).
[25] M. C. Martínez, P. Lava, N. Jachowicz, J. Ryckebusch, K. Vantournhout, and J. M. Udías, Phys. Rev. C **73**, 024607 (2006).
[26] A. V. Butkevich and S. A. Kulagin, Phys. Rev. C **76**, 045502 (2007).
[27] A. Meucci, M. B. Barbaro, J. A. Caballero, C. Giusti, and J. M. Udias, Phys. Rev. Lett. **107**, 172501 (2011).
[28] J. A. Caballero, J. E. Amaro, M. B. Barbaro, T. W. Donnelly, C. Maieron, and J. M. Udias, Phys. Rev. Lett. **95**, 252502 (2005).
[29] J. Amaro, M. Barbaro, J. Caballero, T. Donnelly, and C. Williamson, Phys. Lett. B **696**, 151 (2011).
[30] J. Nieves, I. R. Simo, and M. J. Vicente Vacas, Phys. Rev. C **83**, 045501 (2011).
[31] M. Martini, M. Ericson, and G. Chanfray, Phys. Rev. D **85**, 093012 (2012).
[32] J. Nieves, F. Sanchez, I. R. Simo, and M. J. Vicente Vacas, Phys. Rev. D **85**, 113008 (2012).
[33] O. Lalakulich, U. Mosel, and K. Gallmeister, Phys. Rev. C **86**, 054606 (2012).
[34] T. Sato, D. Uno, and T. S. H. Lee, Phys. Rev. C **67**, 065201 (2003).
[35] E. Hernandez, J. Nieves, and M. Valverde, Phys. Rev. D **76**, 033005 (2007).
[36] E. Hernandez, J. Nieves, M. Valverde, and M. J. Vicente Vacas, Phys. Rev. D **81**, 085046 (2010).
[37] T. Leitner, O. Buss, L. Alvarez-Ruso, and U. Mosel, Phys. Rev. C **79**, 034601 (2009).
[38] B. D. Serot and X. Zhang, Phys. Rev. C **86**, 015501 (2012).
[39] E. Hernández, J. Nieves, and M. J. Vicente Vacas, Phys. Rev. D **87**, 113009 (2013).
[40] S. Ahmad, M. S. Athar, and S. K. Singh, Phys. Rev. D **74**, 073008 (2006).
[41] T. Leitner, O. Buss, U. Mosel, and L. Alvarez-Ruso, Phys. Rev. C **79**, 038501 (2009).
[42] T. Golan, C. Juszczak, and J. T. Sobczyk, Phys. Rev. C **86**, 015505 (2012).
[43] O. Lalakulich and U. Mosel, Phys. Rev. C **87**, 014602 (2013).
[44] S. K. Singh, M. S. Athar, and S. Ahmad, Phys. Rev. Lett. **96**, 241801 (2006).
[45] L. Alvarez-Ruso, L. S. Geng, S. Hirenzaki, and M. J. Vicente Vacas, Phys. Rev. C **75**, 055501 (2007).
[46] J. E. Amaro, E. Hernandez, J. Nieves, and M. Valverde, Phys. Rev. D **79**, 013002 (2009).
[47] S. X. Nakamura, T. Sato, T. S. H. Lee, B. Szczerbinska, and K. Kubodera, Phys. Rev. C **81**, 035502 (2010).
[48] X. Zhang and B. D. Serot, Phys. Rev. C **86**, 035504 (2012).
[49] A. Kartavtsev, E. A. Paschos, and G. J. Gounaris, Phys. Rev. D **74**, 054007 (2006).
[50] C. Berger and L. M. Sehgal, Phys. Rev. D **79**, 053003 (2009).
[51] E. Hernandez, J. Nieves, and M. J. Vicente Vacas, Phys. Rev. D **80**, 013003 (2009).
[52] B. Z. Kopeliovich, I. Schmidt, and M. Siddikov, Phys. Rev. D **85**, 073003 (2012).
[53] C. Athanassopoulos *et al.* (LSND Collaboration), Phys. Rev. Lett. **77**, 3082 (1996).
[54] C. Athanassopoulos *et al.* (LSND Collaboration), Phys. Rev. Lett. **81**, 1774 (1998).
[55] A. A. Aguilar-Arevalo *et al.* (MiniBooNE Collaboration), Phys. Rev. Lett. **110**, 161801 (2013).
[56] A. A. Aguilar-Arevalo *et al.* (MiniBooNE Collaboration), Phys. Rev. Lett. **98**, 231801 (2007).
[57] K. Abe *et al.* (T2K Collaboration), Phys. Rev. D **88**, 032002 (2013).
[58] R. J. Hill, Phys. Rev. D **81**, 013008 (2010).
[59] C. Barbero and A. Mariano, arXiv:1210.6940.
[60] X. Zhang and B. D. Serot, Phys. Lett. B **719**, 409 (2013).
[61] A. M. Ankowski, O. Benhar, T. Mori, R. Yamaguchi, and M. Sakuda, Phys. Rev. Lett. **108**, 052505 (2012).
[62] R. J. Hill, Phys. Rev. D **84**, 017501 (2011).
[63] X. Zhang and B. D. Serot, Phys. Rev. C **86**, 035502 (2012).
[64] T. Leitner, O. Buss, U. Mosel, and L. Alvarez-Ruso, PoS **NUFACT08**, 009 (2008).

[65] T. J. Leitner, Ph.D. thesis, Giessen, 2009.
[66] S. Gershtein, Y. Y. Komachenko, and M. Y. Khlopov, Sov. J. Nucl. Phys. **33**, 860 (1981).
[67] D. Rein and L. Sehgal, Phys. Lett. B **104**, 394 (1981).
[68] L. Alvarez-Ruso, L. S. Geng, and M. J. VicenteVacas, Phys. Rev. C **76**, 068501 (2007).
[69] E. Oset, H. Toki, and W. Weise, Phys. Rep. **83**, 281 (1982).
[70] J. Nieves, E. Oset, and C. Garcia-Recio, Nucl. Phys. A **554**, 554 (1993).
[71] R. Carrasco and E. Oset, Nucl. Phys. A **536**, 445 (1992).
[72] A. Gil, J. Nieves, and E. Oset, Nucl. Phys. A **627**, 543 (1997).
[73] A. Gil, J. Nieves, and E. Oset, Nucl. Phys. A **627**, 599 (1997).
[74] R. Carrasco, J. Nieves, and E. Oset, Nucl. Phys. A **565**, 797 (1993).
[75] S. Hirenzaki, J. Nieves, E. Oset, and M. J. Vicente-Vacas, Phys. Lett. B **304**, 198 (1993).
[76] A. Krutov and V. Troitsky, Eur. Phys. J. A **16**, 285 (2003).
[77] A. Bodek, S. Avvakumov, R. Bradford, and H. S. Budd, Eur. Phys. J. C **53**, 349 (2008).
[78] S. Pate and D. Trujillo, arXiv:1308.5694.
[79] J. Wess and B. Zumino, Phys. Lett. B **37**, 95 (1971).
[80] E. Witten, Nucl. Phys. B **223**, 422 (1983).
[81] O. Lalakulich, E. A. Paschos, and G. Piranishvili, Phys. Rev. D **74**, 014009 (2006).
[82] D. Drechsel, S. Kamalov, and L. Tiator, Eur. Phys. J. A **34**, 69 (2007).
[83] http://www.kph.uni-mainz.de/MAID
[84] S. L. Adler, Ann. Phys. **50**, 189 (1968).
[85] J. Bijtebier, Nucl. Phys. B **21**, 158 (1970).
[86] J. Beringer *et al*. (Particle Data Group), Phys. Rev. D **86**, 010001 (2012).
[87] J. Nieves, M. Valverde, and M. J. Vicente Vacas, Phys. Rev. C **73**, 025504 (2006).
[88] R. Carrasco, E. Oset, and L. Salcedo, Nucl. Phys. A **541**, 585 (1992).
[89] M. Hirata, J. Koch, E. Moniz, and F. Lenz, Ann. Phys. **120**, 205 (1979).
[90] R. Freedman, G. Miller, and E. Henley, Nucl. Phys. A **389**, 457 (1982).
[91] E. Oset and L. Salcedo, Nucl. Phys. A **468**, 631 (1987).
[92] J. Nieves, E. Oset, and C. Garcia-Recio, Nucl. Phys. A **554**, 509 (1993).
[93] S. Singh, M. J. Vicente-Vacas, and E. Oset, Phys. Lett. B **416**, 23 (1998).
[94] J. Lehr, M. Effenberger, and U. Mosel, Nucl. Phys. A **671**, 503 (2000).
[95] E. Hernandez, J. Nieves, and M. Valverde, Phys. Rev. D **82**, 077303 (2010).
[96] P. Fernandez de Cordoba, J. Nieves, E. Oset, and M. J. Vicente-Vacas, Phys. Lett. B **319**, 416 (1993).
[97] P. Fernandez de Cordoba, Y. Ratis, E. Oset, J. Nieves, M. Vicente-Vacas *et al*., Nucl. Phys. A **586**, 586 (1995).
[98] L. Alvarez-Ruso, J. Nieves, I. R. Simo, M. Valverde, and M. J. Vicente Vacas, Phys. Rev. C **87**, 015503 (2013).
[99] R. Eramzhian, M. Gmitro, S. Kamalov, and R. Mach, J. Phys. G **9**, 605 (1983).
[100] D. Drechsel, L. Tiator, S. Kamalov, and S. N. Yang, Nucl. Phys. A **660**, 423 (1999).
[101] S. Boffi, L. Bracci, and P. Christillin, Nuovo Cimento A **104**, 843 (1991).
[102] T. Leitner, U. Mosel, and S. Winkelmann, Phys. Rev. C **79**, 057601 (2009).
[103] C. Garcia-Recio, E. Oset, L. Salcedo, D. Strottman, and M. Lopez, Nucl. Phys. A **526**, 685 (1991).
[104] E. Hernandez, J. Nieves, and M. J. Vicente Vacas (private communication).
[105] A. A. Aguilar-Arevalo *et al*. (MiniBooNE Collaboration), Phys. Rev. Lett. **100**, 032301 (2008).
[106] M. Martini, M. Ericson, and G. Chanfray, Phys. Rev. C **84**, 055502 (2011).
[107] J. Nieves, I. Ruiz Simo, and M. Vicente Vacas, Phys. Lett. B **707**, 72 (2012).
[108] S. Barish, M. Derrick, T. Dombeck, L. Hyman, K. Jaeger *et al*., Phys. Rev. D **19**, 2521 (1979).
[109] G. Radecky, V. Barnes, D. Carmony, A. Garfinkel, M. Derrick *et al*., Phys. Rev. D **25**, 1161 (1982).
[110] T. Kitagaki, H. Yuta, S. Tanaka, A. Yamaguchi, K. Abe *et al*., Phys. Rev. D **34**, 2554 (1986).
[111] T. Kitagaki, H. Yuta, S. Tanaka, A. Yamaguchi, K. Abe *et al*., Phys. Rev. D **42**, 1331 (1990).
[112] C. De Jager, H. De Vries, and C. De Vries, At. Data Nucl. Data Tables **14**, 479 (1974).
[113] J. W. Negele and D. Vautherin, Phys. Rev. C **5**, 1472 (1972).
[114] C. Garcia-Recio, J. Nieves, and E. Oset, Nucl. Phys. A **547**, 473 (1992).
[115] E. Oset, P. Fernandez de Cordoba, L. Salcedo, and R. Brockmann, Phys. Rep. **188**, 79 (1990).
[116] O. Buss, Ph.D. thesis, Giessen, 2008.